

Chapter 1

Double, triple, and n -parton scatterings in high-energy proton and nuclear collisions

David d'Enterria¹ and Alexander Snigirev²

¹*CERN, EP Department, 1211 Geneva, Switzerland*

²*Skobeltsyn Institute of Nuclear Physics, Lomonosov Moscow State University, 119991, Moscow, Russia*

The framework to compute the cross sections for the production of particles with high mass and/or large transverse momentum in double- (DPS), triple- (TPS), and in general n -parton scatterings, from the corresponding single-parton (σ_{SPS}) values in high-energy proton-proton, proton-nucleus, and nucleus-nucleus is reviewed. The basic parameter of the factorized n -parton scattering ansatz is an effective cross section σ_{eff} encoding all unknowns about the underlying generalized n -parton distribution in the proton (nucleon). In its simplest and most economical form, the σ_{eff} parameter can be derived from the transverse parton profile of the colliding protons and/or nucleus, using a Glauber approach. Numerical examples for the cross sections and yields expected for the concurrent DPS or TPS production of heavy-quarks, quarkonia, and/or gauge bosons in proton and nuclear collisions at LHC and Future Circular Collider (FCC) energies are provided. The obtained cross sections are based on perturbative QCD predictions for σ_{SPS} at next-to-leading-order (NLO) or next-to-NLO (NNLO) accuracy including, when needed, nuclear modifications of the corresponding parton densities.

Contents

1. Introduction	2
2. n -parton scattering cross sections in hadron-hadron collisions	3
3. Double and triple parton scattering cross sections in hadron-hadron collisions	5
3.1. TPS cross sections in pp collisions: Numerical examples	8
4. Double and triple parton scattering cross sections in proton-nucleus collisions	10
4.1. DPS cross sections in pA collisions	11
4.2. TPS cross sections in pA collisions	16
5. Double and triple parton scattering cross sections in nucleus-nucleus collisions	21
5.1. DPS cross sections in AA collisions	21
5.2. TPS cross sections in AA collisions	27
6. Summary	29
References	32

1. Introduction

The extended nature of hadrons and their growing parton densities when probed at increasingly higher collision energies, make it possible to simultaneously produce multiple particles with large transverse momentum and/or mass ($\sqrt{p_T^2 + m^2} \gtrsim 2 \text{ GeV}$) in independent multiparton interactions (MPI)¹ in proton-(anti)proton (pp, p \bar{p}),²⁻⁶ as well as in proton-nucleus (pA),⁷⁻¹⁹ and nucleus (AA)^{17,18,20} collisions. Double-, triple-, and in general n -parton scatterings depend chiefly on the transverse overlap of the matter densities of the colliding hadrons, and provide valuable information on (i) the badly-known tridimensional (3D) profile of the partons inside the nucleon, (ii) the unknown energy evolution of the parton density as a function of impact parameter (b), and (iii) the role of multiparton (space, momentum, flavour, colour,...) correlations in the hadronic wave functions. A good understanding of n -parton scattering (NPS) is not only useful to improve our knowledge of the 3D parton structure of the proton, but it is also of relevance for a realistic characterization of backgrounds in searches of new physics in rare final-states with multiple heavy-particles.

The interest in MPI has increased in the last years, not only as a primary source of particle production at hadron colliders,²¹ but also due to their role²² in the “collective” partonic behaviour observed in “central” pp collisions, bearing close similarities to that measured in heavy-ion collisions.^{23,24} As a matter of fact, the larger transverse parton density in a nucleus (with A nucleons) compared to that of a proton, significantly enhances double (DPS) and triple (TPS) parton scattering cross sections coming from interactions where the colliding partons belong to the same or to different nucleons of the nucleus (nuclei), providing thereby additional information on the underlying multiparton dynamics.

Many final-states involving the concurrent production of e.g. heavy-quarks (c, b), quarkonia ($J/\psi, \Upsilon$), jets, and gauge bosons (γ, W, Z) have been measured and found consistent with DPS at the Tevatron (see e.g. early results from CDF^{25,26} and more recent ones from D0^{27,28}) as well as at the LHC (see e.g. the latest results from ATLAS,^{29,30} CMS^{31,32} and LHCb³³). The TPS processes, although not observed so far, have visible cross sections for charm and bottom in pp³⁴ and pA¹⁹ collisions at LHC and future circular (FCC)^{35,36} energies. The present writeup reviews and extends our past work on DPS and TPS in high-energy pp, pA and AA collisions,^{15,17-20,34} expanding the basic factorized formalism to generic NPS processes, and presenting realistic cross section estimates for the double-

Double, triple, and n -parton scatterings in high-energy proton \mathcal{E} nuclear collisions 3

and triple-parton production of heavy-quarks, quarkonia, and/or gauge bosons in proton and nuclear collisions at LHC and FCC.

2. n -parton scattering cross sections in hadron-hadron collisions

In a generic hadronic collision, the inclusive cross section to produce n hard particles in n independent hard parton scatterings, $hh' \rightarrow a_1 \dots a_n$, can be written as a convolution of generalized n -parton distribution functions (PDF) and elementary partonic cross sections summed over all involved partons,

$$\begin{aligned} \sigma_{hh' \rightarrow a_1 \dots a_n}^{\text{NPS}} &= \left(\frac{m}{n!}\right) \sum_{i_1, \dots, i_n, i'_1, \dots, i'_n} \int \Gamma_h^{i_1 \dots i_n}(x_1, \dots, x_n; \mathbf{b}_1, \dots, \mathbf{b}_n; Q_1^2, \dots, Q_n^2) \\ &\quad \times \hat{\sigma}_{a_1}^{i_1 i'_1}(x_1, x'_1, Q_1^2) \cdots \hat{\sigma}_{a_n}^{i_n i'_n}(x_n, x'_n, Q_n^2) \\ &\quad \times \Gamma_{h'}^{i'_1 \dots i'_n}(x'_1, \dots, x'_n; \mathbf{b}_1 - \mathbf{b}, \dots, \mathbf{b}_n - \mathbf{b}; Q_1^2, \dots, Q_n^2) \\ &\quad \times dx_1 \dots dx_n dx'_1, \dots, dx'_n d^2b_1, \dots, d^2b_n d^2b. \end{aligned} \quad (1)$$

Here, $\Gamma_h^{i_1 \dots i_n}(x_1, \dots, x_n; \mathbf{b}_1, \dots, \mathbf{b}_n; Q_1^2, \dots, Q_n^2)$ are n -parton generalized distribution functions, depending on the momentum fractions x_1, \dots, x_n , and energy scales Q_1, \dots, Q_n , at transverse positions $\mathbf{b}_1, \dots, \mathbf{b}_n$ of the i_1, \dots, i_n partons, producing final-state particles a_1, \dots, a_n with subprocess cross sections $\hat{\sigma}_{a_1}^{i_1 i'_1}, \dots, \hat{\sigma}_{a_n}^{i_n i'_n}$. The combinatorial $(m/n!)$ prefactor takes into account the different cases of (indistinguishable or not) final states. For a set of identical particles (i.e. when $a_1 = \dots = a_n$) we have $m = 1$, whereas $m = 2, 3, 6, \dots$ for final-states with an increasing number of different particles produced. In the particular cases of interest here, we have

- DPS: $m = 1$ if $a_1 = a_2$; and $m = 2$ if $a_1 \neq a_2$.
- TPS: $m = 1$ if $a_1 = a_2 = a_3$; $m = 3$ if $a_1 = a_2$, or $a_1 = a_3$, or $a_2 = a_3$; and $m = 6$ if $a_1 \neq a_2 \neq a_3$.

The n -parton distribution function $\Gamma_h^{i_1 \dots i_n}(x_1, \dots, x_n; \mathbf{b}_1, \dots, \mathbf{b}_n; Q_1^2, \dots, Q_n^2)$ theoretically encodes all the 3D parton structure information of the hadron of relevance to compute the NPS cross sections, including the density of partons in the transverse plane and any intrinsic partonic correlations in kinematical and/or quantum-numbers spaces. Since $\Gamma_h^{i_1 \dots i_n}$ is potentially a very complicated object, one often resorts to simplified alternatives to compute NPS cross sections based on simpler quantities. As a matter of

fact, without any loss of generality, any n -parton cross section can be always expressed in a more economical and phenomenologically useful form in terms of single-parton scattering (SPS) inclusive cross sections, theoretically calculable in perturbative quantum chromodynamics (pQCD) approaches through collinear factorization³⁷ as a function of “standard” (longitudinal) PDF, $D_h^i(x, Q^2)$, at a given order of accuracy in the QCD coupling expansion (next-to-next-to-leading order, NNLO, being the current state-of-the-art for most calculations):

$$\sigma_{hh' \rightarrow a}^{\text{SPS}} = \sum_{i_1, i_2} \int D_h^{i_1}(x_1; Q_1^2) \hat{\sigma}_a^{i_1 i_2}(x_1, x_1') D_{h'}^{i_2}(x_1'; Q_1^2) dx_1 dx_1'. \quad (2)$$

More precisely, any n -parton cross section can be expressed as the n th-product of the corresponding SPS cross sections for the production of each single final-state particle, normalized by the $(n-1)$ power of an effective cross section,

$$\sigma_{hh' \rightarrow a_1 \dots a_n}^{\text{NPS}} = \left(\frac{m}{n!} \right) \frac{\sigma_{hh' \rightarrow a_1}^{\text{SPS}} \dots \sigma_{hh' \rightarrow a_n}^{\text{SPS}}}{\sigma_{\text{eff, NPS}}^{n-1}}, \quad (3)$$

where $\sigma_{\text{eff, NPS}}$ encodes all the unknowns related to the underlying generalized PDF. Equation (3) encapsulates the intuitive result that the probability to produce n particles in a given inelastic hadron-hadron collision should be proportional to the n -product of probabilities to independently produce each one of them, normalized by the $n-1$ power of an effective cross section to guarantee the proper units of the final result (3).^a

The value of $\sigma_{\text{eff, NPS}}$ in Eq. (3) can be theoretically estimated making a few common approximations. First, the n -PDF are commonly assumed to be factorizable in terms of longitudinal and transverse components, i.e.

$$\begin{aligned} \Gamma_h^{i_1 \dots i_n}(x_1, \dots, x_n; \mathbf{b}_1, \dots, \mathbf{b}_n; Q_1^2, \dots, Q_n^2) \\ = D_h^{i_1 \dots i_n}(x_1, \dots, x_n; Q_1^2, \dots, Q_n^2) \cdot f(\mathbf{b}_1) \dots f(\mathbf{b}_n), \end{aligned} \quad (4)$$

where $f(\mathbf{b}_1)$ describes the transverse parton density of the hadron, often considered a universal function for all types of partons, from which the

^aIndeed, in the simplest DPS case, the probability to produce particles a, b in a pp collision is: $P_{\text{pp} \rightarrow ab} = P_{\text{pp} \rightarrow a} \cdot P_{\text{pp} \rightarrow b} = \frac{\sigma_{\text{pp} \rightarrow a}}{\sigma_{\text{pp}}^{\text{inel}}} \cdot \frac{\sigma_{\text{pp} \rightarrow b}}{\sigma_{\text{pp}}^{\text{inel}}}$, which implies: $\sigma_{\text{pp} \rightarrow a, b} = \frac{\sigma_{\text{pp} \rightarrow a} \cdot \sigma_{\text{pp} \rightarrow b}}{\sigma_{\text{eff}}}$, with $\sigma_{\text{eff}} \approx \sigma_{\text{pp}}^{\text{inel}}$. In reality, the measured value of $\sigma_{\text{eff}} \approx 15$ mb is a factor of 2–3 lower (i.e. the DPS probability is 2–3 times *larger*) than the naive $\sigma_{\text{eff}} \approx \sigma_{\text{pp}}^{\text{inel}}$ expectation for typical “hard” (minijet) inelastic pp partonic cross sections $\sigma_{\text{pp}}^{\text{inel}} \approx 30$ –50 mb. This is so because the independent-scattering assumption does not hold as the probability to produce a second particle is higher in low-impact-parameter (large transverse overlap) pp events where a first partonic scattering has already taken place.

Double, triple, and n-parton scatterings in high-energy proton & nuclear collisions 5

corresponding hadron-hadron overlap function can be derived:

$$T(\mathbf{b}) = \int f(\mathbf{b}_1)f(\mathbf{b}_1 - \mathbf{b})d^2b_1, \quad (5)$$

with the fixed normalization $\int T(\mathbf{b})d^2b = 1$. Making the further assumption that the longitudinal components reduce to the product of independent single PDF,

$$D_h^{i_1 \dots i_n}(x_1, \dots, x_n; Q_1^2, \dots, Q_n^2) = D_h^{i_1}(x_1; Q_1^2) \dots D_h^{i_n}(x_n; Q_n^2), \quad (6)$$

the effective NPS cross section bears a simple geometric interpretation in terms of powers of the inverse of the integral of the hadron-hadron overlap function over all impact parameters,

$$\sigma_{\text{eff,NPS}} = \left\{ \int d^2b T^n(\mathbf{b}) \right\}^{-1/(n-1)}. \quad (7)$$

3. Double and triple parton scattering cross sections in hadron-hadron collisions

The generalized expression (1) for the case of double-parton-scattering cross sections in hadron-hadron collisions, $hh' \rightarrow a_1 a_2$, reads

$$\begin{aligned} \sigma_{hh' \rightarrow a_1 a_2}^{\text{DPS}} &= \left(\frac{m}{2}\right) \sum_{i,j,k,l} \int \Gamma_h^{ij}(x_1, x_2; \mathbf{b}_1, \mathbf{b}_2; Q_1^2, Q_2^2) \\ &\quad \times \hat{\sigma}_{a_1}^{ik}(x_1, x'_1, Q_1^2) \cdot \hat{\sigma}_{a_2}^{jl}(x_2, x'_2, Q_2^2) \\ &\quad \times \Gamma_{h'}^{kl}(x'_1, x'_2; \mathbf{b}_1 - \mathbf{b}, \mathbf{b}_2 - \mathbf{b}; Q_1^2, Q_2^2) \\ &\quad \times dx_1 dx_2 dx'_1 dx'_2 d^2b_1 d^2b_2 d^2b. \end{aligned} \quad (8)$$

Applying the “master” equations (3) and (7) for $n = 2$, one can express this cross section as a double product of independent single inclusive cross sections

$$\sigma_{hh' \rightarrow a_1 a_2}^{\text{DPS}} = \left(\frac{m}{2}\right) \frac{\sigma_{hh' \rightarrow a_1}^{\text{SPS}} \cdot \sigma_{hh' \rightarrow a_2}^{\text{SPS}}}{\sigma_{\text{eff,DPS}}}, \quad (9)$$

where the effective DPS cross section (7) that normalizes the double SPS product is

$$\sigma_{\text{eff,DPS}} = \left[\int d^2b T^2(\mathbf{b}) \right]^{-1}. \quad (10)$$

Similarly, the generic expression (1) for the TPS cross section for the process $hh' \rightarrow a_1 a_2 a_3$ reads³⁸

$$\begin{aligned} \sigma_{hh' \rightarrow a_1 a_2 a_3}^{\text{TPS}} &= \left(\frac{m}{3!}\right) \sum_{i,j,k,l,m,n} \int \Gamma_h^{ijk}(x_1, x_2, x_3; \mathbf{b}_1, \mathbf{b}_2, \mathbf{b}_3; Q_1^2, Q_2^2, Q_3^2) \\ &\quad \times \hat{\sigma}_{a_1}^{il}(x_1, x'_1, Q_1^2) \cdot \hat{\sigma}_{a_2}^{jm}(x_2, x'_2, Q_2^2) \cdot \hat{\sigma}_{a_3}^{kn}(x_3, x'_3, Q_3^2) \\ &\quad \times \Gamma_{h'}^{lmn}(x'_1, x'_2, x'_3; \mathbf{b}_1 - \mathbf{b}, \mathbf{b}_2 - \mathbf{b}, \mathbf{b}_3 - \mathbf{b}; Q_1^2, Q_2^2, Q_3^2) \\ &\quad \times dx_1 dx_2 dx_3 dx'_1 dx'_2 dx'_3 d^2 b_1 d^2 b_2 d^2 b_3 d^2 b. \end{aligned} \quad (11)$$

which can be reduced to a triple product of independent single inclusive cross sections

$$\sigma_{hh' \rightarrow a_1 a_2 a_3}^{\text{TPS}} = \left(\frac{m}{3!}\right) \frac{\sigma_{hh' \rightarrow a_1}^{\text{SPS}} \cdot \sigma_{hh' \rightarrow a_2}^{\text{SPS}} \cdot \sigma_{hh' \rightarrow a_3}^{\text{SPS}}}{\sigma_{\text{eff,TPS}}^2}, \quad (12)$$

normalized by the *square* of an effective TPS cross section (7), that amounts to³⁴

$$\sigma_{\text{eff,TPS}}^2 = \left[\int d^2 b T^3(\mathbf{b}) \right]^{-1}, \quad (13)$$

One can estimate the values of the effective DPS (10) and TPS (13) cross sections via Eq. (5) for different transverse parton profiles of the colliding hadrons, such as those typically implemented in the modern pp Monte Carlo (MC) event generators PYTHIA 8,³⁹ and HERWIG++.⁴⁰ In PYTHIA 8, the pp overlap function as a function of impact parameter is often parametrized in the form:

$$T(\mathbf{b}) = \frac{m}{2\pi r_p^2 \Gamma(2/m)} \exp[-(b/r_p)^m], \quad (14)$$

normalized to one, $\int T(\mathbf{b}) d^2 b = 1$, where r_p is the characteristic “radius” of the proton, Γ is the gamma function, and the exponent m depends on the MC “tune” obtained from fits to the measured underlying-event activity and various DPS cross sections in pp collisions.³² It varies between a pure Gaussian ($m = 2$) to a more peaked exponential-like ($m = 0.7, 1$) distribution. From the corresponding integrals of the square and cube of $T(\mathbf{b})$, we obtain:

$$\sigma_{\text{eff,DPS}} = \left(\int d^2 b T^2(\mathbf{b}) \right)^{-1} = 2\pi r_p^2 \frac{2^{2/m} \Gamma(2/m)}{m}, \quad \text{and} \quad (15)$$

$$\sigma_{\text{eff,TPS}} = \left(\int d^2 b T^3(\mathbf{b}) \right)^{-1/2} = 2\pi r_p^2 \frac{3^{1/m} \Gamma(2/m)}{m}. \quad (16)$$

Double, triple, and n-parton scatterings in high-energy proton & nuclear collisions 7

From Eq. (15), in order to reproduce the experimental $\sigma_{\text{eff,DPS}} \simeq 15 \pm 5$ mb value extracted in multiple DPS measurements at Tevatron^{25–28} and LHC,^{5,29–33} the characteristic proton “radius” parameter amounts to $r_p \simeq 0.11 \pm 0.02, 0.24 \pm 0.04, 0.49 \pm 0.08$ fm for exponents $m = 0.7, 1, 2$ as defined in Eq. (14). The values of $\sigma_{\text{eff,DPS}}$ and $\sigma_{\text{eff,TPS}}$, Eqs. (15)–(16), are of course closely related: $\sigma_{\text{eff,TPS}} = (3/4)^{1/m} \cdot \sigma_{\text{eff,DPS}}$. Such a relationship is independent of the exact numerical value of the proton “size” r_p , but depends on the overall shape of its transverse profile characterized by the exponent m . For typical PYTHIA-8 $m = 0.7, 1, 2$ exponents tuned from experimental data,³² one obtains $\sigma_{\text{eff,TPS}} = [0.66, 0.75, 0.87] \times \sigma_{\text{eff,DPS}}$ respectively.

The HERWIG++ event generator uses an alternative parametrization of the proton profile described by the dipole fit of the two-gluon form factor in the momentum representation⁴¹

$$F_{2g}(\mathbf{q}) = 1/(q^2/m_g^2 + 1)^2, \quad (17)$$

where the gluon mass m_g parameter characterizes the transverse momentum q distribution of the proton, and the transverse density is obtained from its Fourier-transform: $f(\mathbf{b}) = \int e^{-i\mathbf{b}\cdot\mathbf{q}} F_{2g}(\mathbf{q}) \frac{d^2q}{(2\pi)^2}$. The corresponding DPS (10) and TPS (13) effective cross sections read:⁴⁰

$$\sigma_{\text{eff,DPS}} = \left[\int F_{2g}^4(q) \frac{d^2q}{(2\pi)^2} \right]^{-1} = \frac{28\pi}{m_g^2}, \quad (18)$$

and³⁴

$$\begin{aligned} \sigma_{\text{eff,TPS}} = & \left[\int (2\pi)^2 \delta(\mathbf{q}_1 + \mathbf{q}_2 + \mathbf{q}_3) F_{2g}(\mathbf{q}_1) F_{2g}(\mathbf{q}_2) F_{2g}(\mathbf{q}_3) \right. \\ & \left. \times F_{2g}(-\mathbf{q}_1) F_{2g}(-\mathbf{q}_2) F_{2g}(-\mathbf{q}_3) \frac{d^2q_1}{(2\pi)^2} \frac{d^2q_2}{(2\pi)^2} \frac{d^2q_3}{(2\pi)^2} \right]^{-1/2}. \end{aligned}$$

Numerically integrating the latter and combining it with (18), we obtain $\sigma_{\text{eff,TPS}} = 0.83 \times \sigma_{\text{eff,DPS}}$, which is quite close to the value derived for the Gaussian pp overlap function in PYTHIA 8. In order to reproduce the experimentally measured $\sigma_{\text{eff,DPS}} \simeq 15 \pm 5$ mb values, the characteristic proton “size” for this parametrization amounts to $r_g = 1/m_g \simeq 0.13 \pm 0.02$ fm.

Despite the wide range of proton transverse parton densities and associated effective radius parameters considered, we find that the $\sigma_{\text{eff,TPS}} \lesssim \sigma_{\text{eff,DPS}}$ result is robust with respect to the underlying parton profile. As a matter of fact, from the average and standard deviation of all typical

parton transverse distributions studied in Ref.,³⁴ the following relationship between double and triple scattering effective cross sections can be derived:

$$\sigma_{\text{eff,TPS}} = k \times \sigma_{\text{eff,DPS}}, \text{ with } k = 0.82 \pm 0.11. \quad (19)$$

Thus, from the typical $\sigma_{\text{eff,DPS}} \simeq 15 \pm 5$ value extracted from a wide range of DPS measurements at Tevatron and LHC, the following numerical effective TPS cross section is finally obtained:

$$\sigma_{\text{eff,TPS}} = 12.5 \pm 4.5 \text{ mb}. \quad (20)$$

3.1. TPS cross sections in pp collisions: Numerical examples

Many theoretical and experimental studies exist that have extracted $\sigma_{\text{eff,DPS}}$ from computed and/or measured DPS cross sections for a large variety of final-states in pp collisions.⁴² In this subsection, we focus therefore on the TPS case for which we presented the first-ever estimates in Ref.³⁴ The experimental observation of triple parton scatterings in pp collisions requires perturbatively-calculable processes with SPS cross sections not much smaller than $\mathcal{O}(1 \mu\text{b})$ since, otherwise, the corresponding TPS cross sections (which go as the cube of the SPS values) are extremely reduced. Indeed, according to Eq. (12) with the data-driven estimate (20), a triple hard process $pp \rightarrow a a a$, with SPS cross sections $\sigma_{pp \rightarrow a}^{\text{SPS}} \approx 1 \mu\text{b}$, has a very small cross section $\sigma_{pp \rightarrow a a a}^{\text{TPS}} \approx 1 \text{ fb}$. Evidence for TPS appears thereby challenging already without accounting for additional reducing factors arising from decay branching ratios, and experimental acceptances and reconstruction inefficiencies, of the produced particles. Promising processes to probe TPS, with not too small pQCD cross sections, are inclusive charm ($pp \rightarrow c\bar{c} + X$), and bottom ($pp \rightarrow b\bar{b} + X$), whose cross sections are dominated by gluon-gluon fusion ($gg \rightarrow q\bar{q}$) at small x , for which one can expect a non-negligible contributions of DPS^{43–45} and TPS^{19,34,46} to their total inclusive production (Fig. 1).

The TPS heavy-quark cross sections can be computed with Eq. (12) for $m = 1$, i.e. $\sigma_{pp \rightarrow q\bar{q}}^{\text{TPS}} = (\sigma_{pp \rightarrow q\bar{q}}^{\text{SPS}})^3 / (6 \sigma_{\text{eff,TPS}}^2)$ with $\sigma_{\text{eff,TPS}}$ given by (20), and $\sigma_{pp \rightarrow q\bar{q}}^{\text{SPS}}$ calculated via Eq. (2) at NNLO accuracy using a modified version⁴⁷ of the Top++ (v2.0) code,⁴⁸ with $N_f = 3, 4$ light flavors, heavy-quark pole masses set at $m_{c,b} = 1.67, 4.66 \text{ GeV}$, default renormalization and factorization scales set at $\mu_R = \mu_F = 2 m_{c,b}$, and using the ABMP16 proton PDF.⁴⁹ Such NNLO calculations increase the total SPS heavy-quark cross sections by up to 20% at LHC energies compared to the corresponding NLO results,^{50,51} reaching a better agreement with the experimental data,

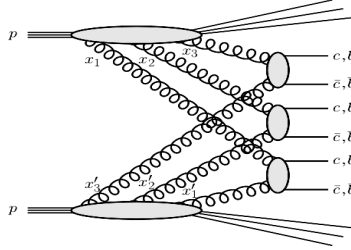
Double, triple, and n -parton scatterings in high-energy proton \mathcal{E} nuclear collisions 9

Fig. 1. Schematic diagram for the leading order contribution to triple charm ($c\bar{c}$) and bottom ($b\bar{b}$) pair production via gluon fusion, in TPS processes in pp collisions.

and featuring much reduced scale uncertainties ($\pm 50\%$, $\pm 15\%$ for $c\bar{c}$, $b\bar{b}$).⁴⁷ Figure 2 shows the resulting total SPS and TPS cross sections for charm and bottom production over $\sqrt{s} = 35 \text{ GeV} - 100 \text{ TeV}$, and Table 1 lists the results with associated uncertainties for the nominal pp c.m. energies at LHC and FCC. The PDF uncertainties are obtained from the corresponding 28 eigenvalues of the ABMP16 set. The dominant uncertainty comes from the theoretical scales dependence, which is estimated by modifying μ_R and μ_F within a factor of two.

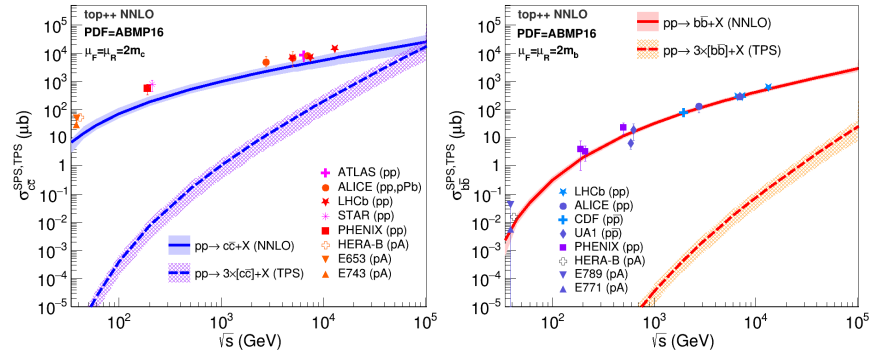


Fig. 2. Total charm (left) and bottom (right) cross sections in pp collisions as a function of c.m. energy, in single-parton (solid line) and triple-parton (dashed line) parton scatterings. Bands around curves indicate scale, PDF (and $\sigma_{\text{eff},\text{TPS}}$, in the case of σ^{TPS}) uncertainties added in quadrature. The symbols are experimental data collected in.⁴⁷

Figure 2 shows that the TPS cross sections rise fast with \sqrt{s} , as the cube of the corresponding SPS cross sections. Triple- $c\bar{c}$ production from three independent parton scatterings amounts to 5% of the inclusive charm yields at the LHC ($\sqrt{s} = 14 \text{ TeV}$) and to more than half of the total

Table 1. Cross sections for charm and bottom production in SPS (NNLO) and TPS processes in pp collisions at LHC and FCC energies. The quoted uncertainties include scales (sc), PDF, and total (quadratic, including $\sigma_{\text{eff,TPS}}$) values.

Final state	$\sqrt{s} = 14$ TeV	$\sqrt{s} = 100$ TeV
$\sigma_{c\bar{c}+X}^{\text{SPS}}$	$7.1 \pm 3.5_{\text{sc}} \pm 0.3_{\text{PDF}}$ mb	$25.0 \pm 16.0_{\text{sc}} \pm 1.3_{\text{PDF}}$ mb
$\sigma_{c\bar{c}c\bar{c}+X}^{\text{TPS}}$	$0.39 \pm 0.28_{\text{tot}}$ mb	$16.7 \pm 11.8_{\text{tot}}$ mb
$\sigma_{b\bar{b}+X}^{\text{SPS}}$	$0.56 \pm 0.09_{\text{sc}} \pm 0.01_{\text{PDF}}$ mb	$2.8 \pm 0.6_{\text{sc}} \pm 0.1_{\text{PDF}}$ mb
$\sigma_{b\bar{b}b\bar{b}+X}^{\text{TPS}}$	$0.19 \pm 0.12_{\text{tot}}$ μb	$24 \pm 17_{\text{tot}}$ μb

charm cross section at the FCC. Since the total pp inelastic cross section at $\sqrt{s} = 100$ TeV is $\sigma_{\text{pp}} \simeq 105$ mb,⁵² charm-anticharm triplets are expected to be produced in $\sim 15\%$ of the pp collisions at these energies. Triple- $b\bar{b}$ cross sections remain quite small and reach only about 1% of the inclusive bottom cross section at FCC(100 TeV). These results indicate that TPS is experimentally observable in triple heavy-quark pair final-states at the LHC and FCC. The possibility of detecting triple charm-meson production in pp collisions at the LHC has been discussed in more detail in Ref.⁴⁶

4. Double and triple parton scattering cross sections in proton-nucleus collisions

In proton-nucleus collisions, the parton flux is enhanced by the number A of nucleons in the nucleus and the SPS cross section is simply expected to be that of proton-proton collisions or, more exactly, that of proton-nucleon collisions (pN, with $N = p, n$ being *bound* protons and neutrons with their appropriate relative fractions in the nucleus) taking into (anti)shadowing modifications of the nuclear PDF,⁵³ scaled by the factor A , i.e.⁵⁴

$$\sigma_{\text{pA} \rightarrow a}^{\text{SPS}} = \sigma_{\text{pN} \rightarrow a}^{\text{SPS}} \int d^2b T_{\text{pA}}(\mathbf{b}) = A \cdot \sigma_{\text{pN} \rightarrow a}^{\text{SPS}}. \quad (21)$$

Here, $T_{\text{pA}}(\mathbf{r})$ is the standard nuclear thickness function, analogous to Eq. (5) for the pp case, as a function of the impact parameter \mathbf{r} between the colliding proton and nucleus, given by an integral of the nuclear density function $\rho_A(\mathbf{r})$ over the longitudinal direction

$$T_{\text{pA}}(\mathbf{r}) = \int \rho_A(\sqrt{r^2 + z^2}) dz, \text{ normalized to } \int T_{\text{pA}}(\mathbf{r}) d^2r = A, \quad (22)$$

which can be easily computed using (simplified) analytical nuclear profiles, and/or employing realistic Fermi-Dirac (aka. Woods-Saxon) nuclear spatial densities determined in elastic eA measurements,⁵⁵ via a MC Glauber model.⁵⁴

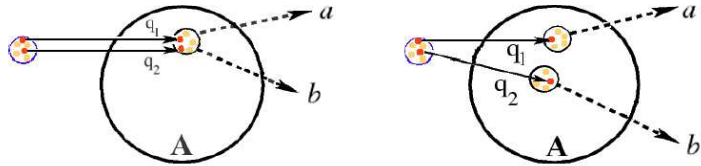
The most naive assumption is to consider that the NPS cross sections in pA collisions can be obtained by simply A -scaling the corresponding pp NPS values, as done via Eq. (21) for the SPS cross sections. We show next that DPS and TPS cross sections in proton-nucleus collisions can be significantly enhanced, with extra $A^{4/3}$ (for DPS and TPS) and $A^{5/3}$ (for TPS alone) terms complementing the A -scaling, due to additional multiple scattering probabilities among partons from different nucleons.

4.1. DPS cross sections in pA collisions

The larger transverse parton density in nuclei compared to protons results in enhanced DPS cross sections, $pA \rightarrow ab$, coming from interactions where the two partons of the nucleus belong to (1) the same nucleon, and (2) two different nucleons^{7–15} as shown in Fig. 3. Namely,

$$\sigma_{pA}^{\text{DPS}} = \sigma_{pA}^{\text{DPS},1} + \sigma_{pA}^{\text{DPS},2}, \quad (23)$$

where



$$\sigma_{pA \rightarrow ab}^{\text{DPS},1} = A \cdot \sigma_{pN \rightarrow ab}^{\text{DPS}} \quad \sigma_{pA \rightarrow ab}^{\text{DPS},2} \approx \sigma_{pN \rightarrow ab}^{\text{DPS}} \cdot \sigma_{\text{eff,DPS}} \cdot T_{AA}(0)$$

Fig. 3. Schematic diagrams of double-parton scatterings contributions in pA collisions where the two colliding partons belong to the same (left) or a different (right) pair of nucleons in the nucleus. The corresponding cross sections are described in the text.

- (1) The first term is just the A -scaled DPS cross section in pN collisions:

$$\sigma_{pA \rightarrow ab}^{\text{DPS},1} = A \cdot \sigma_{pN \rightarrow ab}^{\text{DPS}}, \quad (24)$$

- (2) the second contribution, from parton interactions from two different nucleons, depends on the square of T_{pA} ,

$$\sigma_{pA \rightarrow ab}^{\text{DPS},2} = \sigma_{pN \rightarrow ab}^{\text{DPS}} \cdot \sigma_{\text{eff,DPS}} \cdot F_{pA}, \quad (25)$$

$$\text{with } F_{pA} = \frac{A-1}{A} \int T_{pA}^2(\mathbf{r}) d^2r = (A-1)/A \cdot T_{AA}(0), \quad (26)$$

where the $(A-1)/A$ factor accounts for the difference between the number of nucleon pairs and the number of *different* nucleon pairs, and

$T_{AA}(0)$ is the nuclear overlap function at $b = 0$ for the corresponding AA collision. In the simplest approximation of a spherical nucleus with uniform nucleon density with radius $R_A \propto A^{1/3}$, the factor (26) can be written as

$$F_{pA} = \frac{9A(A-1)}{8\pi R_A^2} \approx \frac{A^{4/3}}{14\pi} [\text{mb}^{-1}]. \quad (27)$$

where the second approximate equality (valid for large A) indicates the corresponding dependence on the A mass-number alone. For Pb, with $A = 208$ and $R_A \approx 7 \text{ fm} \approx 22 \text{ mb}^{1/2}$, one obtains $F_{pA} \approx 31.5 \text{ mb}^{-1}$, in good agreement with the more accurate result, $F_{pA} = 30.25 \text{ mb}^{-1}$, computed with a Glauber MC⁵⁴ using the standard Woods-Saxon spatial density of the lead nucleus (radius $R_A = 6.36 \text{ fm}$, and surface thickness $a = 0.54 \text{ fm}$).⁵⁵

The sum of (24) and (25) yields the inclusive cross section for the DPS production of particles a and b in a pA collision:

$$\sigma_{pA \rightarrow ab}^{\text{DPS}} = A \cdot \sigma_{pN \rightarrow ab}^{\text{DPS}} [1 + \sigma_{\text{eff,DPS}} F_{pA}/A] \quad (28)$$

$$\approx A \cdot \sigma_{pN \rightarrow ab}^{\text{DPS}} \left[1 + \frac{\sigma_{\text{eff,DPS}}}{14[\text{mb}]\pi} A^{1/3} \right], \quad (29)$$

which is enhanced by the factor in parentheses compared to the A -scaled DPS cross section in pN collisions. Given the experimental $\sigma_{\text{eff,DPS}} \approx 15 \text{ mb}$ value, the pp-to-pA DPS enhancement factor can be further numerically simplified as $[1 + A^{1/3}/\pi]$, which goes from ~ 1.4 for small to ~ 3 for large nuclei. Namely, the relative weight of the two DPS terms of Eq. (29) goes from $\sigma_{pA \rightarrow ab}^{\text{DPS},1} : \sigma_{pA \rightarrow ab}^{\text{DPS},2} = 0.7 : 0.3$ (small A) to $0.33 : 0.66$ (large A). Thus, e.g. in the case of pPb collisions, 33% of the DPS yields come from partonic interactions within just one nucleon of the Pb nucleus, whereas 66% of them involve parton scatterings from two different Pb nucleons.

The final factorized DPS formula in proton-nucleus collisions can be written as a function of the elementary proton-nucleon single-parton cross sections as

$$\sigma_{pA \rightarrow ab}^{\text{DPS}} = \left(\frac{m}{2} \right) \frac{\sigma_{pN \rightarrow a}^{\text{SPS}} \cdot \sigma_{pN \rightarrow b}^{\text{SPS}}}{\sigma_{\text{eff,DPS,pA}}}, \quad (30)$$

where the effective DPS pA cross section in the denominator depends on the effective cross section measured in pp, and on a pure geometric quantity (F_{pA}) that is directly derivable from the well-known nuclear transverse profile, namely

$$\sigma_{\text{eff,DPS,pA}} = \frac{\sigma_{\text{eff,DPS}}}{A + \sigma_{\text{eff,DPS}} F_{pA}} \approx \frac{\sigma_{\text{eff,DPS}}}{A + \sigma_{\text{eff,DPS}} T_{AA}(0)} \approx \frac{\sigma_{\text{eff,DPS}}}{A + A^{4/3}/\pi}. \quad (31)$$

Double, triple, and n-parton scatterings in high-energy proton & nuclear collisions 13

For a Pb nucleus (with $A = 208$, and $F_{\text{pA}} = 30.25 \text{ mb}^{-1}$) and taking $\sigma_{\text{eff,DPS}} = 15 \pm 5 \text{ mb}$, one obtains $\sigma_{\text{eff,DPS,pA}} = 22.5 \pm 2.3 \text{ } \mu\text{b}$. The overall increase of DPS cross sections in pA compared to pp collisions is $\sigma_{\text{eff,DPS}}/\sigma_{\text{eff,DPS,pA}} \approx [A + A^{4/3}/\pi]$ which, in the case of pPb implies a factor of ~ 600 relative to pp (ignoring nuclear PDF effects here), i.e. a factor of $[1 + A^{1/3}/\pi] \approx 3$ higher than the naive expectation assuming the same A -scaling of the single-parton cross sections, Eq. (21). One can thus exploit such large expected DPS signals over the SPS backgrounds in proton-nucleus collisions to study double parton scatterings in detail and, in particular, to extract the value of $\sigma_{\text{eff,DPS}}$ independently of measurements in pp collisions—given that the parameter F_{pA} in Eq. (31) depends on the comparatively better-known transverse density of nuclei.

DPS cross sections in pA collisions: Numerical examples

One of the “cleanest” channels to study DPS in pp collisions is same-sign WW production⁵⁶ as it features precisely-known pQCD SPS cross sections, a clean experimental final-state with two like-sign leptons plus missing transverse momentum from the undetected neutrinos, and small non-DPS backgrounds^b. The DPS cross section in pPb for same-sign WW production was first estimated in Ref.,¹⁵ computing the SPS W^\pm cross sections ($\sigma_{\text{pN} \rightarrow W}^{\text{SPS}}$) with MCFM (v.6.2)^{57,58} at NLO accuracy with CT10 proton⁵⁹ and EPS09 nuclear⁶⁰ PDF, and setting default renormalisation and factorisation theoretical scales to $\mu = \mu_R = \mu_F = m_W$. The background $W^\pm W^\pm \text{jj}$ cross sections are computed with MCFM for the QCD part (formally at LO, but setting $\mu_R = \mu_F = 150 \text{ GeV}$ to effectively account for missing higher-order corrections), and with VBFNLO (v.2.6)^{61,62} for the electroweak contributions with theoretical scales set to the momentum transfer of the exchanged boson, $\mu^2 = t_{W,Z}$. In pPb at 8.8 TeV, the EPS09 nuclear PDF modifies the total W^+ (W^-) production cross section by about -7% ($+15\%$) compared to that obtained using the free proton CT10 PDF.⁶³

We extend here the results of Ref.,¹⁵ using Eq. (30) with $m = 1$ and $\sigma_{\text{eff,DPS,pA}} = 22.5 \pm 2.3 \text{ } \mu\text{b}$, and including FCC pPb energies ($\sqrt{s_{\text{NN}}} = 63 \text{ TeV}$). The resulting cross sections are listed in Table 2. The uncertainties of the SPS NLO single-W cross sections amount to about

^bThe lowest order at which two same-sign W bosons can be produced is accompanied with two jets ($W^\pm W^\pm \text{jj}$), $q q \rightarrow W^\pm W^\pm q' q'$ with $q = u, c, \dots$ and $q' = d, s, \dots$ whose leading contributions are $\mathcal{O}(\alpha_s^2 \alpha_w^2)$ for the mixed QCD-electroweak diagrams, and $\mathcal{O}(\alpha_w^4)$ for the pure vector-boson fusion (VBF) processes, where α_w is the electroweak coupling.

$\pm 10\%$ by adding in quadrature those from the EPS09 PDF eigenvector sets (the proton PDF uncertainties are much lower in the relevant x, Q^2 regions) and from the theoretical scales (obtained by independently varying μ_R and μ_F within a factor of two). The QCD $W^\pm W^\pm jj$ cross sections uncertainties are those from the full-NLO calculations,⁶⁴ whereas those of the VBF cross sections are much smaller as they do not involve any gluons in the initial state. The DPS cross section uncertainties are dominated by a propagated $\pm 30\%$ uncertainty from $\sigma_{\text{eff,DPS}}$.

Table 2. Cross sections for the production of single-W, and same-sign W pairs in pPb collisions at LHC and FCC c.m. energies, computed at NLO with MCFM and VBFNLO for the processes quoted. The last column lists the same-sign DPS cross sections (sum of positive and negative W pairs) obtained with Eq. (30) for $\sigma_{\text{eff,DPS,pA}} = 22.5 \pm 2.3 \mu\text{b}$.

pPb	W ⁺ , W ⁻	W ⁺ W ⁺ jj (QCD), (VBF)	W [±] W [±] (DPS)
	NLO (μb)	NLO (pb)	(pb)
5.0 TeV	$6.85 \pm 0.68, 5.88 \pm 0.59$	$12.1 \pm 1.2, 12.4 \pm 0.6$	44 ± 13
8.8 TeV	$12.6 \pm 1.3, 11.1 \pm 1.1$	$40.4 \pm 4.0, 51.8 \pm 2.0$	152 ± 45
63 TeV	$83.4 \pm 8.4, 77.9 \pm 7.8$	$166. \pm 17., 2150. \pm 220.$	$6700. \pm 2000.$

Figure 4 shows the computed total cross sections for all W processes considered over the c.m. energy $\sqrt{s_{\text{NN}}} = 2\text{--}65$ TeV range. At the nominal LHC pPb c.m. energy of 8.8 TeV, the same-sign WW DPS cross section is $\sigma_{\text{pPb} \rightarrow \text{WW}}^{\text{DPS}} \approx 150$ pb (thick curve), larger than the sum of SPS backgrounds, $\sigma_{\text{pPb} \rightarrow \text{WWjj}}^{\text{SPS}}$ (lowest dashed curve) obtained adding the QCD and electroweak cross sections for the production of W^+W^+ (W^-W^-) plus 2 jets. In the fully-leptonic final-state ($W^\pm W^\pm \rightarrow \ell\nu \ell'\nu'$, with $\ell = e^\pm, \mu^\pm$) and accounting for decay branching ratios and standard ATLAS/CMS acceptance and reconstruction cuts ($|y^\ell| < 2.5, p_T^\ell > 15$ GeV), one expects up to 10 DPS same-sign WW events in $\mathcal{L}_{\text{int}} = 2 \text{ pb}^{-1}$ integrated luminosity.¹⁵ At FCC energies ($\sqrt{s_{\text{NN}}} = 63$ TeV), the ssWW DPS cross section is more than twice larger than the ssWW(jj) SPS one. With $\mathcal{L}_{\text{int}} \approx 30 \text{ pb}^{-1}$, and a factor twice larger rapidity coverage,³⁶ one expects $\mathcal{O}(10^4)$ ssWW pairs from DPS processes. Same-sign WW production in pPb collisions constitutes thereby a promising channel to measure $\sigma_{\text{eff,DPS}}$, independently of the standard pp-based extractions of this quantity.

Table 3 collects the estimated DPS cross sections for the combined production of quarkonia ($J/\psi, \Upsilon$) and/or electroweak bosons (W, Z) in pPb collisions at the nominal LHC energy of $\sqrt{s_{\text{NN}}} = 8.8$ TeV. The quoted SPS pN cross sections have been obtained at NLO accuracy with

Double, triple, and n -parton scatterings in high-energy proton & nuclear collisions 15

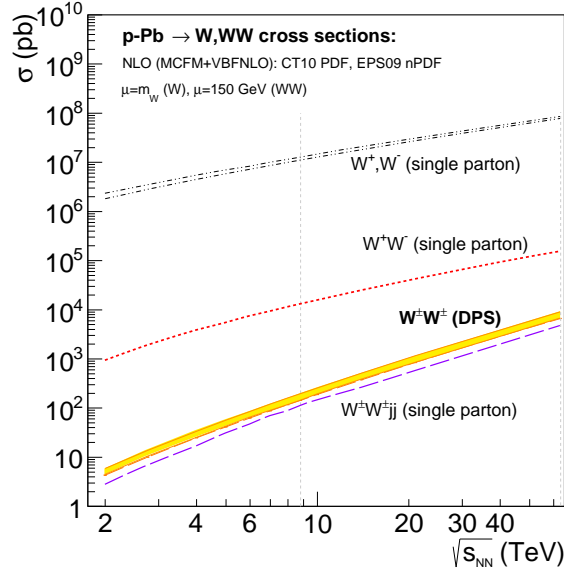


Fig. 4. Cross sections as a function of c.m. energy for single-W, and W-pair (both opposite-sign and same-sign) production from single-parton and from double-parton scatterings in pPb collisions. Dotted vertical lines indicate the nominal 8.8 and 63 TeV pPb energies at LHC and FCC.

Table 3. Production cross sections at $\sqrt{s_{NN}} = 8.8$ TeV for SPS quarkonia and electroweak bosons in pN collisions, and for DPS double- J/ψ , $J/\psi + \Upsilon$, $J/\psi + W$, $J/\psi + Z$, double- Υ , $\Upsilon + W$, $\Upsilon + Z$, and same-sign WW, in pPb. DPS cross sections are obtained via Eq. (30) for $\sigma_{\text{eff,DPS,pA}} = 22.5 \mu\text{b}$ (uncertainties, not quoted, are of the order of 30%), and the corresponding yields, after dilepton decays and acceptance+efficiency losses (note that the J/ψ yields are *per unit of rapidity* at mid- and forward- y , see text), are given for the nominal 1 pb^{-1} integrated luminosity.

pPb (8.8 TeV)	$J/\psi + J/\psi$	$J/\psi + \Upsilon$	$J/\psi + W$	$J/\psi + Z$
$\sigma_{\text{pN} \rightarrow a}^{\text{SPS}}, \sigma_{\text{pN} \rightarrow b}^{\text{SPS}}$	45 μb ($\times 2$)	45 μb , 2.6 μb	45 μb , 60 nb	45 μb , 35 nb
$\sigma_{\text{pPb}}^{\text{DPS}}$	45 μb	5.2 μb	120 nb	70 nb
$N_{\text{pPb}}^{\text{DPS}} (1 \text{ pb}^{-1})$	~ 65	~ 60	~ 15	~ 3
	$\Upsilon + \Upsilon$	$\Upsilon + W$	$\Upsilon + Z$	ss WW
$\sigma_{\text{pN} \rightarrow a}^{\text{SPS}}, \sigma_{\text{pN} \rightarrow b}^{\text{SPS}}$	2.6 μb ($\times 2$)	2.6 μb , 60 nb	2.6 μb , 35 nb	60 nb ($\times 2$)
$\sigma_{\text{pPb}}^{\text{DPS}}$	150 nb	7 nb	4 nb	150 pb
$N_{\text{pPb}}^{\text{DPS}} (1 \text{ pb}^{-1})$	~ 15	~ 8	~ 1.5	~ 4

the color evaporation model (CEM)⁶⁵ for quarkonia (see details in Section 5.1), and with MCFM for the electroweak bosons, using CT10 proton and EPS09 nuclear PDF. The DPS cross sections are estimated via Eq. (30) with $\sigma_{\text{eff,DPS,pA}} = 22.5 \mu\text{b}$, and the visible DPS yields are quoted for $\mathcal{L}_{\text{int}} = 1 \text{ pb}^{-1}$ integrated luminosities, taking into account the branching fractions $\text{BR}(J/\psi, \Upsilon, W, Z) = 6\%, 2.5\%, 11\%, 3.4\%$ per dilepton decay; plus simplified acceptance and efficiency losses: $\mathcal{A} \times \mathcal{E}(J/\psi) \approx 0.01$ (over 1-unit of rapidity at $|y| = 0$, and $|y| = 2$), and $\mathcal{A} \times \mathcal{E}(\Upsilon; W, Z) \approx 0.2; 0.5$ (over $|y| < 2.5$). All listed processes are in principle observable in the LHC proton-lead runs, whereas rarer DPS processes like $W+Z$ and $Z+Z$ have much lower cross sections and require much higher luminosities and/or c.m. energies such as those reachable at the FCC.

4.2. TPS cross sections in pA collisions

Similarly to the DPS case, the proton-nucleus TPS cross section for the $pA \rightarrow abc$ process, is obtained from the sum of three contributions:

$$\sigma_{pA}^{\text{TPS}} = \sigma_{pA}^{\text{TPS},1} + \sigma_{pA}^{\text{TPS},2} + \sigma_{pA}^{\text{TPS},3}, \text{ with} \quad (32)$$

- (1) A cross section, scaling like Eq. (21) for the SPS case, corresponding to the TPS value in pN collisions scaled by A , namely:

$$\sigma_{pA \rightarrow abc}^{\text{TPS},1} = A \cdot \sigma_{pN \rightarrow abc}^{\text{TPS}}. \quad (33)$$

- (2) A second contribution, involving interactions of partons from two different nucleons in the nucleus, depending on the square of T_{pA} ,

$$\sigma_{pA \rightarrow abc}^{\text{TPS},2} = \sigma_{pN \rightarrow abc}^{\text{TPS}} \cdot 3 \frac{\sigma_{\text{eff,TPS}}^2}{\sigma_{\text{eff,DPS}}} F_{pA}, \quad (34)$$

with F_{pA} given by Eq. (26).

- (3) A third term, involving interactions among partons from three different nucleons, depending on the cube of T_{pA} ,

$$\sigma_{pA \rightarrow abc}^{\text{TPS},3} = \sigma_{pN \rightarrow abc}^{\text{TPS}} \cdot \sigma_{\text{eff,TPS}}^2 \cdot C_{pA}, \text{ with} \quad (35)$$

$$C_{pA} = \frac{(A-1)(A-2)}{A^2} \int d^2b T_{pA}^3(\mathbf{b}), \quad (36)$$

with the $(A-1)(A-2)/A^2$ factor introduced to take into account the difference between the total number of nucleon TPS and that of *different* nucleon TPS. By using a hard-sphere approximation for a nucleus of radius $R_A \propto A^{1/3}$, the C_{pA} factor can be analytically calculated as

$$C_{pA} = \frac{27}{4} \frac{A(A-1)(A-2)}{5\pi^2 R_A^4} \approx \frac{A^{5/3}}{160\pi^2} [\text{mb}^{-2}], \quad (37)$$

Double, triple, and n-parton scatterings in high-energy proton & nuclear collisions 17

where the last approximate equality holds for large A . For a Pb nucleus ($A = 208$, $R_A = 22 \text{ mb}^{1/2}$) this factor amounts to $C_{pA} \approx 5.1 \text{ mb}^{-2}$, in agreement with the $C_{pA} = 4.75 \text{ mb}^{-2}$ numerically obtained through a Glauber MC with a realistic Woods-Saxon Pb profile.

The inclusive TPS cross section for the independent production of three particles a , b , and c in pA collisions is obtained from the sum of the three terms (33), (34), and (35):

$$\sigma_{pA \rightarrow abc}^{\text{TPS}} = A \sigma_{pN \rightarrow abc}^{\text{TPS}} \left[1 + 3 \frac{\sigma_{\text{eff,TPS}}^2 F_{pA}}{\sigma_{\text{eff,DPS}} A} + \sigma_{\text{eff,TPS}}^2 \frac{C_{pA}}{A} \right] \quad (38)$$

$$\approx A \sigma_{pN \rightarrow abc}^{\text{TPS}} \left[1 + \frac{\sigma_{\text{eff,TPS}}^2}{\sigma_{\text{eff,DPS}}} \frac{3 A^{1/3}}{14[\text{mb}]\pi} + \sigma_{\text{eff,TPS}}^2 \frac{A^{2/3}}{160[\text{mb}^2]\pi^2} \right], \quad (39)$$

where the last approximation holds for large A , and can be written as a function of $\sigma_{\text{eff,TPS}}$ and A alone making use of Eq. (19):

$$\sigma_{pA \rightarrow abc}^{\text{TPS}} \approx A \sigma_{pN \rightarrow abc}^{\text{TPS}} \left[1 + \sigma_{\text{eff,TPS}} \frac{A^{1/3}}{5.7[\text{mb}]\pi} + \sigma_{\text{eff,TPS}}^2 \frac{A^{2/3}}{160[\text{mb}^2]\pi^2} \right]. \quad (40)$$

The TPS cross section in pA collisions is enhanced by the factor in parentheses in Eqs. (38)–(40) compared to the corresponding one in pN collisions scaled by A . The final formula for TPS in proton-nucleus reads

$$\sigma_{pA \rightarrow abc}^{\text{TPS}} = \left(\frac{m}{6} \right) \frac{\sigma_{pN \rightarrow a}^{\text{SPS}} \cdot \sigma_{pN \rightarrow b}^{\text{SPS}} \cdot \sigma_{pN \rightarrow c}^{\text{SPS}}}{\sigma_{\text{eff,TPS,pA}}^2}, \quad (41)$$

where the effective TPS pA cross section in the denominator depends on the effective TPS cross section measured in pp, and on purely geometric quantities (F_{pA} , C_{pA}) directly derivable from the well-known nuclear profiles,¹⁹

$$\sigma_{\text{eff,TPS,pA}} = \left[\frac{A}{\sigma_{\text{eff,TPS}}^2} + \frac{3 F_{pA}[\text{mb}^{-1}]}{\sigma_{\text{eff,DPS}}} + C_{pA}[\text{mb}^{-2}] \right]^{-1/2} \quad (42)$$

which can be numerically approximated as a function of the number A of nucleons in the nucleus (for A large) alone, as follows

$$\sigma_{\text{eff,TPS,pA}} \approx \left[\frac{A}{\sigma_{\text{eff,TPS}}^2} + \frac{A^{4/3}}{5.7[\text{mb}]\pi \sigma_{\text{eff,TPS}}} + \frac{A^{5/3}}{160[\text{mb}^2]\pi^2} \right]^{-1/2}. \quad (43)$$

For a Pb nucleus ($A = 208$, $F_{pA} = 30.25 \text{ mb}^{-1}$, and $C_{pA} = 4.75 \text{ mb}^{-2}$) and taking $\sigma_{\text{eff,TPS}} = 12.5 \pm 4.5 \text{ mb}$, the effective TPS cross section amounts to $\sigma_{\text{eff,TPS,pA}} = 0.29 \pm 0.04 \text{ mb}$. Thus, for pPb the relative importance of the

three TPS terms of Eq. (38) is $\sigma_{pA \rightarrow abc}^{\text{TPS},1} : \sigma_{pA \rightarrow abc}^{\text{TPS},2} : \sigma_{pA \rightarrow abc}^{\text{TPS},3} = 1 : 4.54 : 3.56$. Namely, in pPb collisions, 10% of the TPS yields come from partonic interactions within just one nucleon of the lead nucleus, 50% involve scatterings within two nucleons, and 40% come from partonic interactions in three different Pb nucleons. The sum of the three contributions in Eq. (38), ignoring differences between pN and pp collisions, indicates that the TPS cross sections in pPb are about nine times larger than the naive expectation based on A -scaling of the corresponding pN TPS cross sections, Eq. (33). One can thus exploit the large expected TPS signals in proton-nucleus collisions to extract the $\sigma_{\text{eff,TPS}}$ parameter, and thereby $\sigma_{\text{eff,DPS}}$ via Eq. (19), independently of TPS measurements in pp collisions—given that the F_{pA} and C_{pA} parameters in Eq. (38) depend on the comparatively better known transverse density of nuclei.

TPS cross sections in pA collisions: Numerical examples

As a concrete numerical example in Ref.¹⁹ we have computed the TPS cross sections for charm ($c\bar{c}$) and bottom ($b\bar{b}$) production, following the motivation for the similar measurement in pp collisions (Section 3.1), over a wide range of c.m. energies, $\sqrt{s_{\text{NN}}} \approx 5\text{--}500$ TeV, of relevance for collider (LHC and FCC) and ultra-high-energy cosmic rays physics. The TPS heavy-quark cross sections are computed via Eq. (41) for $m = 1$, i.e. $\sigma_{pA \rightarrow c\bar{c}, b\bar{b}}^{\text{TPS}} = (\sigma_{pN \rightarrow c\bar{c}, b\bar{b}}^{\text{SPS}})^3 / (6 \sigma_{\text{eff,TPS,pA}}^2)$ with the effective TPS cross sections given by Eq. (42): $\sigma_{\text{eff,TPS,pA}} = 0.29 \pm 0.04$ mb for pPb, and $\sigma_{\text{eff,TPS,pA}} = 2.2 \pm 0.4$ mb for p-Air collisions^c. The SPS cross sections, $\sigma_{pN \rightarrow c\bar{c}, b\bar{b}}^{\text{SPS}}$, are calculated at NNLO via Eq. (2) with Top++ (v.2.0) with the same setup as described in Sec. 3.1, using the ABMP16 proton and EPS09 nuclear PDF. In the pPb case, the inclusion of EPS09 nuclear shadowing reduces moderately the total charm and bottom cross sections in pN compared to pp collisions, by about 10% (15%) and 5% (10%) at the LHC (FCC). At $\sqrt{s_{\text{NN}}} = 5.02$ TeV, our prediction ($\sigma_{p\text{Pb} \rightarrow c\bar{c}}^{\text{SPS,NNLO}} = 650 \pm 290_{\text{sc}} \pm 60_{\text{PDF}}$ mb) agrees well with the ALICE total D-meson measurement⁶⁶ extrapolated using FONLL⁵⁰ to a total charm cross section of $\sigma_{p\text{Pb} \rightarrow c\bar{c}}^{\text{ALICE}} = 640 \pm 60_{\text{stat}} \pm 60_{\text{syst}}^{+60}_{-110}$ mb (data point in the top-left panel of Fig. 5). Since the TPS pPb cross section go as the cube of $\sigma_{pN \rightarrow c\bar{c}}^{\text{SPS}}$, the impact of shadowing is amplified and leads to 15–35% depletions of the TPS cross sections compared to results obtained with the free proton PDF.

^cUsing $A = 14.3$ for a 78%–21% mixture of ^{14}N – ^{16}O , with $F_{pA} = 0.51$ mb⁻¹, and $C_{pA} = 0.016$ mb⁻² obtained via a Glauber MC.⁵⁴

Double, triple, and n-parton scatterings in high-energy proton & nuclear collisions 19

Table 4. Cross sections for inclusive inelastic, and for SPS and TPS charm and bottom production in pPb (at LHC and FCC energies) and p-Air (at GZK-cutoff c.m. energies) collisions. For the SPS and TPS cross sections the quoted values include scales, PDF, and total (quadratically added, including $\sigma_{\text{eff,TPS}}$) uncertainties. [The asterisk indicates that the theoretical prediction of the TPS charm cross section is “unphysical” (see text).]

Process	pPb(8.8 TeV)	pPb(63 TeV)	p-Air(430 TeV)
$\sigma_{\text{pA}}^{\text{inel}}$	2.2 ± 0.4 b	2.4 ± 0.4 mb	0.61 ± 0.10 b
$\sigma_{c\bar{c}+X}^{\text{SPS}}$	$0.96 \pm 0.45_{\text{sc}} \pm 0.10_{\text{PDF}}$ b	$3.4 \pm 1.9_{\text{sc}} \pm 0.4_{\text{PDF}}$ b	$0.75 \pm 0.5_{\text{sc}} \pm 0.1_{\text{PDF}}$ b
$\sigma_{c\bar{c}c\bar{c}c\bar{c}+X}^{\text{TPS}}$	$200 \pm 140_{\text{tot}}$ mb	$8.7^* \pm 6.2_{\text{tot}}$ b	$5.0^* \pm 3.6_{\text{tot}}$ b
$\sigma_{b\bar{b}+X}^{\text{SPS}}$	$72 \pm 12_{\text{sc}} \pm 5_{\text{PDF}}$ mb	$370 \pm 75_{\text{sc}} \pm 30_{\text{PDF}}$ mb	$110 \pm 25_{\text{sc}} \pm 5_{\text{PDF}}$ mb
$\sigma_{b\bar{b}b\bar{b}b\bar{b}+X}^{\text{TPS}}$	$0.084 \pm 0.045_{\text{tot}}$ μb	$11 \pm 7_{\text{tot}}$ μb	$17 \pm 11_{\text{tot}}$ μb

Table 4 collects the total inelastic and the heavy-quarks cross sections at $\sqrt{s_{\text{NN}}} = 8.8$ TeV and 63 TeV in pPb collisions, and at $\sqrt{s_{\text{NN}}} = 430$ TeV in p-Air collisions. The latter c.m. energy corresponds to the so-called “GZK cutoff”^{67,68} reached in collisions of $\mathcal{O}(10^{20}$ eV) proton cosmic-rays, with N and O nuclei at rest in the upper atmosphere. The PDF uncertainties include those from the proton and nucleus in quadrature, as obtained from the corresponding $28 \oplus 30$ eigenvalues of the ABMP16 \oplus EPS09 sets. The dominant uncertainty is linked to the theoretical scale choice, estimated by modifying μ_R and μ_F within a factor of two. At the LHC, the large SPS $c\bar{c}$ cross section (~ 1 b) results in triple- $c\bar{c}$ cross sections from independent parton scatterings amounting to about 20% of the inclusive charm yields. Since the total inelastic pPb cross sections is $\sigma_{\text{pPb}}^{\text{inel}} \approx 2.2$ b, charm TPS takes place in about 10% of the pPb events at 8.8 TeV. At the FCC, the theoretical TPS charm cross section even overcomes the inclusive charm one. Such an unphysical result indicates that quadruple, quintuple,... parton-parton scatterings are expected to produce extra $c\bar{c}$ pairs with non-negligible probability. The huge TPS $c\bar{c}$ cross sections in pPb at $\sqrt{s_{\text{NN}}} = 63$ TeV, will make triple- J/ψ production, with $\sigma(J/\psi J/\psi J/\psi + X) \approx 1$ mb, observable. Triple- $b\bar{b}$ cross sections remain comparatively small, in the 0.1 mb range, at the LHC but reach ~ 10 mb (i.e. 3% of the total inclusive bottom cross section) at the FCC.

Figure 5 plots the cross sections over $\sqrt{s_{\text{NN}}} \approx 40$ GeV–500 TeV for SPS (solid bands), TPS (dashed bands) for charm (left) and bottom (right) production, and total inelastic (dotted curve) in pPb (top panels) and p-Air (bottom panels) collisions. Whenever the central value of the theoretical TPS cross section overcomes the inclusive charm cross section, indicative of multiple (beyond three) $c\bar{c}$ -pair production, we equalize it to the latter. At

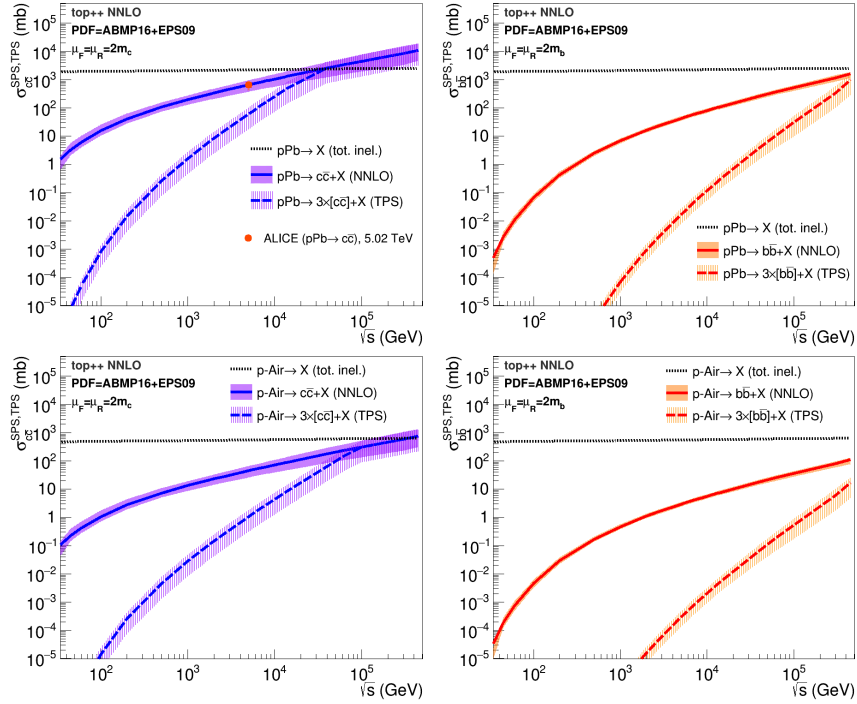


Fig. 5. Charm (left) and bottom (right) cross sections in pPb (top panels) and p-Air (bottom panels) collisions as a function of c.m. energy, in single-parton (solid band) and triple-parton (dashed band) scatterings, compared to the total inelastic pA cross sections (dotted line in all panels). Bands around curves indicate scale, PDF (and $\sigma_{\text{eff,TPS}}$ in the TPS case) uncertainties added in quadrature. The pPb $\rightarrow c\bar{c} + X$ charm data point on the top-left plot has been derived from the ALICE D-meson data.⁶⁶

$\sqrt{s_{\text{NN}}} \approx 25$ TeV, the total charm and inelastic pPb cross sections are equal implying that, above this c.m. energy, *all* pPb interactions produce at least three charm pairs. In the $b\bar{b}$ case, such a situation only occurs at much higher c.m. energies, above 500 TeV. For p-Air collisions at the GZK cut-off, the cross section for inclusive as well as TPS charm production equals the total inelastic cross section ($\sigma_{\text{pAir}}^{\text{inel}} \approx 0.61$ b) indicating that *all* p-Air collisions produce at least three $c\bar{c}$ -pairs in multiple partonic interactions. In the $b\bar{b}$ case, about 20% of the p-Air collisions produce bottom hadrons, but only about 4% of them have TPS production. These results emphasize the numerical importance of TPS processes in proton-nucleus collisions at colliders, and their relevance for hadronic MC models commonly used for the simulation of ultrarelativistic cosmic-ray interactions with the atmo-

Double, triple, and n-parton scatterings in high-energy proton & nuclear collisions 21

sphere⁶⁹ which, so far, do not include any heavy-quark production.

5. Double and triple parton scattering cross sections in nucleus-nucleus collisions

In nucleus-nucleus collisions, the parton flux is enhanced by A nucleons in each nucleus, and the SPS cross section is simply expected to be that of NN collisions, taking into account (anti)shadowing effects in the nuclear PDF, scaled by the factor A^2 , i.e.⁵⁴

$$\sigma_{AA \rightarrow a}^{\text{SPS}} = \int T_{AA}(\mathbf{b}) d^2b = A^2 \cdot \sigma_{NN \rightarrow a}^{\text{SPS}}. \quad (44)$$

where $T_{AA}(\mathbf{b})$ the standard nuclear overlap function, normalized to A^2 ,

$$T_{AA}(\mathbf{b}) = \int T_{pA}(\mathbf{b}_1) T_{pA}(\mathbf{b}_1 - \mathbf{b}) d^2b_1 d^2b, \quad (45)$$

with $T_{pA}(\mathbf{b})$ being the nuclear thickness function at impact parameter \mathbf{b} , Eq. (22), connecting the centres of the colliding nucleus in the transverse plane. In the next two subsections, we present the estimates for DPS and TPS cross sections in AA collisions from the corresponding SPS values.

5.1. DPS cross sections in AA collisions

The DPS cross section in AA is the sum of three terms, corresponding to the diagrams of Fig. 6,

$$\sigma_{AA}^{\text{DPS}} = \sigma_{AA}^{\text{DPS},1} + \sigma_{AA}^{\text{DPS},2} + \sigma_{AA}^{\text{DPS},3}, \text{ where} \quad (46)$$

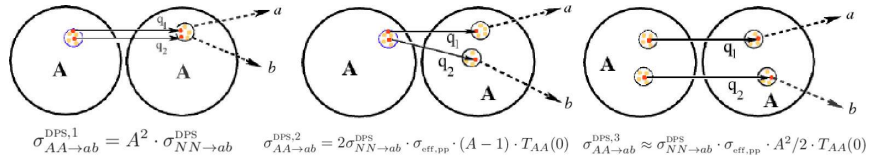


Fig. 6. Schematic diagrams contributing to DPS cross sections in AA collisions: The two colliding partons belong to the same pair of nucleons (left), partons from one nucleon in one nucleus collide with partons from two different nucleons in the other nucleus (center), and the two colliding partons belong to two different nucleons from both nuclei (right).

- (1) The first term, similarly to the SPS cross sections Eq. (44), is just the DPS cross section in NN collisions scaled by A^2 ,

$$\sigma_{AA \rightarrow ab}^{\text{DPS},1} = A^2 \cdot \sigma_{NN \rightarrow ab}^{\text{DPS}}. \quad (47)$$

- (2) The second term accounts for interactions of partons from one nucleon in one nucleus with partons from two different nucleons in the other nucleus,

$$\sigma_{AA \rightarrow ab}^{\text{DPS},2} = 2\sigma_{NN \rightarrow ab}^{\text{DPS}} \cdot \sigma_{\text{eff,DPS}} \cdot A \cdot F_{\text{pA}}, \quad (48)$$

with $F_{\text{pA}} \approx T_{\text{AA}}(0)$ given by Eq. (26).

- (3) The third contribution from interactions of partons from two different nucleons in one nucleus with partons from two different nucleons in the other nucleus, reads

$$\sigma_{AA \rightarrow ab}^{\text{DPS},3} = \sigma_{NN \rightarrow ab}^{\text{DPS}} \cdot \sigma_{\text{eff,DPS}} \cdot T_{3,\text{AA}} \text{ with}, \quad (49)$$

$$T_{3,\text{AA}} = \left(\frac{A-1}{A}\right)^2 \int T_{\text{pA}}(\mathbf{b}_1) T_{\text{pA}}(\mathbf{b}_2) T_{\text{pA}}(\mathbf{b}_1 - \mathbf{b}) T_{\text{pA}}(\mathbf{b}_2 - \mathbf{b}) d^2 b_1 d^2 b_2 d^2 b \quad (50)$$

$$= \left(\frac{A-1}{A}\right)^2 \int d^2 r T_{\text{AA}}^2(\mathbf{r}) \approx \frac{A^2}{2} \cdot T_{\text{AA}}(0), \quad (51)$$

where the latter integral of the nuclear overlap function squared does not depend much on the precise shape of the transverse parton density in the nucleus, amounting to $A^2/1.94 \cdot T_{\text{AA}}(0)$ for a hard-sphere and $A^2/2 \cdot T_{\text{AA}}(0)$ for a Gaussian profile. The factor $((A-1)/A)^2$ takes into account the difference between the number of nucleon pairs and the number of *different* nucleon pairs.

Adding (47), (48), and (49), the inclusive cross section of a DPS process with two hard parton subprocesses a and b in AA collisions can be written as

$$\sigma_{AA \rightarrow ab}^{\text{DPS}} = A^2 \sigma_{NN \rightarrow ab}^{\text{DPS}} \left[1 + \frac{2}{A} \sigma_{\text{eff,DPS}} F_{\text{pA}} + \frac{(A-1)^2}{A^2} \sigma_{\text{eff,DPS}} \int d^2 r T_{\text{AA}}^2(\mathbf{r}) \right] \quad (52)$$

$$\approx A^2 \sigma_{NN \rightarrow ab}^{\text{DPS}} \left[1 + \frac{2}{A} \sigma_{\text{eff,DPS}} T_{\text{AA}}(0) + \frac{1}{2} \sigma_{\text{eff,DPS}} T_{\text{AA}}(0) \right] \quad (53)$$

$$\approx A^2 \sigma_{NN \rightarrow ab}^{\text{DPS}} \left[1 + \frac{\sigma_{\text{eff,DPS}}}{7_{[\text{mb}]} \pi} A^{1/3} + \frac{\sigma_{\text{eff,DPS}}}{28_{[\text{mb}]} \pi} A^{4/3} \right], \quad (54)$$

where the last approximation, showing the A -dependence of the DPS cross sections, applies for large nuclei. The factor in parentheses in Eqs. (52)–(54) indicates the enhancement in DPS cross sections in AA compared to the corresponding A^2 -scaled values in nucleon-nucleon collisions, Eq. (47), which amounts to ~ 27 (for small $A = 40$) or ~ 215 (for large $A = 208$). The overall mass-number scaling of DPS cross sections in AA compared to pp collisions is given by a $(A^2 + k A^{7/3} + w A^{10/3})$ factor with $k, w \approx 0.7, 0.2$,

Double, triple, and n-parton scatterings in high-energy proton & nuclear collisions 23

which is clearly dominated numerically by the $A^{10/3}$ term. The final DPS cross section “pocket formula” in heavy-ion collisions can be written as

$$\sigma_{AA \rightarrow ab}^{\text{DPS}} = \left(\frac{m}{2} \right) \frac{\sigma_{NN \rightarrow a}^{\text{SPS}} \cdot \sigma_{NN \rightarrow b}^{\text{SPS}}}{\sigma_{\text{eff,DPS,AA}}}, \quad (55)$$

with the effective AA normalization cross section amounting to

$$\sigma_{\text{eff,DPS,AA}} \approx \frac{1}{A^2 \left[\sigma_{\text{eff,DPS}}^{-1} + \frac{2}{A} T_{AA}(0) + \frac{1}{2} T_{AA}(0) \right]}. \quad (56)$$

For a value of $\sigma_{\text{eff,DPS}} \approx 15$ mb and for nuclei with mass numbers $A = 40$ – 240 , we find that the relative weights of the three components contributing to DPS scattering in AA collisions are $1 : 2.3 : 23$ (for $A = 40$) and $1 : 4 : 200$ (for $A = 208$). Namely, only 13% (for $^{40}\text{Ca}+^{40}\text{Ca}$) or 2.5% (for $^{208}\text{Pb}+^{208}\text{Pb}$) of the DPS yields in AA collisions come from the first two diagrams of Fig. 6 involving partons from one single nucleon. Clearly, the “pure” DPS contributions arising from partonic collisions within a single nucleon (first and second terms of Eq. (54)) are much smaller than the last term from double particle production coming from two independent *nucleon-nucleon* collisions. The DPS cross sections in AA are practically unaffected by the value of $\sigma_{\text{eff,DPS}}$, but dominated instead by double-parton interactions from *different nucleons* in both nuclei. In the case of ^{208}Pb - ^{208}Pb collisions, the numerical value of Eq. (56) is $\sigma_{\text{eff,DPS,AA}} = 1.5 \pm 0.1$ nb, with uncertainties dominated by those of the Glauber MC determination of $T_{AA}(0)$. Whereas the single-parton cross sections in PbPb collisions, Eq. (44), are enhanced by a factor of $A^2 \simeq 4 \cdot 10^4$ compared to that in pp collisions, the corresponding double-parton cross sections are enhanced by a much higher factor of $\sigma_{\text{eff,DPS}} / \sigma_{\text{eff,DPS,AA}} \propto 0.2 A^{10/3} \simeq 10^7$.

Centrality dependence of DPS cross sections in AA collisions

The DPS cross sections discussed above are for “minimum bias” AA collisions without any selection in reaction centrality. The cross sections for single and double-parton scattering within an impact-parameter interval $[b_1, b_2]$, corresponding to a given centrality percentile $f_{\%}$ of the total AA cross section $\sigma_{AA}^{\text{inel}}$, with average nuclear overlap function $\langle T_{AA}[b_1, b_2] \rangle$ read (for large A , so that $A - 1 \approx A$):

$$\sigma_{AA[b_1, b_2] \rightarrow a}^{\text{SPS}} = A^2 \sigma_{NN \rightarrow a}^{\text{SPS}} f_1[b_1, b_2] = \sigma_{NN \rightarrow a}^{\text{SPS}} \cdot f_{\%} \sigma_{AA}^{\text{inel}} \cdot \langle T_{AA}[b_1, b_2] \rangle, \quad (57)$$

$$\begin{aligned} \sigma_{AA[b_1, b_2] \rightarrow ab}^{\text{DPS}} &= A^2 \sigma_{NN \rightarrow ab}^{\text{DPS}} f_1[b_1, b_2] \times \\ &\times \left[1 + \frac{2\sigma_{\text{eff,DPS}}}{A} T_{AA}(0) \frac{f_2[b_1, b_2]}{f_1[b_1, b_2]} + \sigma_{\text{eff,DPS}} T_{AA}(0) \frac{f_3[b_1, b_2]}{f_1[b_1, b_2]} \right], \quad (58) \end{aligned}$$

where the latter has been obtained integrating Eq. (52) over $b_1 < b < b_2$, and where the three dimensionless and appropriately-normalized fractions f_1 , f_2 , and f_3 are:

$$f_1[b_1, b_2] = \frac{2\pi}{A^2} \int_{b_1}^{b_2} b db T_{AA}(b) = \frac{f_{\%} \sigma_{AA}^{\text{inel}}}{A^2} \langle T_{AA}[b_1, b_2] \rangle,$$

$$f_2[b_1, b_2] = \frac{2\pi}{A T_{AA}(0)} \int_{b_1}^{b_2} b db \int d^2 b_1 T_{pA}(\mathbf{b}_1) T_{pA}(\mathbf{b}_1 - \mathbf{b}) T_{pA}(\mathbf{b}_1 - \mathbf{b}),$$

$$f_3[b_1, b_2] = \frac{2\pi}{A^2 T_{AA}(0)} \int_{b_1}^{b_2} b db T_{AA}^2(b).$$

The integrals f_2 , and f_3 can be evaluated⁷⁰ for small enough centrality bins around a given impact parameter b . The dominant f_3/f_1 contribution in Eq. (58) is simply given by the ratio $\langle T_{AA}[b_1, b_2] \rangle / T_{AA}(0)$ which is practically insensitive (except for very peripheral collisions) to the precise shape of the nuclear density profile. The second centrality-dependent DPS term, f_2/f_1 , cannot be expressed in a simple form in terms of $T_{AA}(b)$, but it is of order unity for the most central collisions, $f_2/f_1 = 4/3$, and $16/15$ for Gaussian and hard-sphere profiles respectively, and it is suppressed in comparison with the third leading term by an extra factor $\sim 2/A$. Finally, for not very-peripheral collisions ($f_{\%} \lesssim 0-65\%$), the DPS cross section in a (thin) impact-parameter $[b_1, b_2]$ range can be approximated by

$$\sigma_{AA \rightarrow ab}^{\text{DPS}}[b_1, b_2] \approx \sigma_{NN \rightarrow ab}^{\text{DPS}} \cdot \sigma_{\text{eff,DPS}} \cdot f_{\%} \sigma_{AA}^{\text{inel}} \cdot \langle T_{AA}[b_1, b_2] \rangle^2 \quad (59)$$

$$= \left(\frac{m}{2}\right) \sigma_{NN \rightarrow a}^{\text{SPS}} \cdot \sigma_{NN \rightarrow b}^{\text{SPS}} \cdot f_{\%} \sigma_{AA}^{\text{inel}} \cdot \langle T_{AA}[b_1, b_2] \rangle^2. \quad (60)$$

Dividing this last expression by Eq. (57), one finally obtains the corresponding ratio of double- to single-parton-scattering cross sections as a function of impact parameter^d:

$$\left(\sigma_{AA \rightarrow ab}^{\text{DPS}} / \sigma_{AA \rightarrow a}^{\text{SPS}}\right)[b_1, b_2] \approx \left(\frac{m}{2}\right) \sigma_{NN \rightarrow b}^{\text{SPS}} \cdot \langle T_{AA}[b_1, b_2] \rangle. \quad (61)$$

DPS cross sections in AA collisions: Numerical examples

Quarkonia has been historically considered a sensitive probe of the quark-gluon-plasma (QGP) formed in heavy-ion collisions,⁷¹ and thereby their production channels need to be theoretically and experimentally well understood in pp, pA and AA collisions.⁷² Double-quarkonium ($J/\psi J/\psi$,

^dSuch analytical expression neglects the first and second terms of Eq. (58). In the $f_{\%} \approx 65-100\%$ centrality percentile, the second term would add about 20% more DPS cross-sections, and for very peripheral collisions ($f_{\%} \approx 85-100\%$, where $\langle T_{AA}[b_1, b_2] \rangle$ is of order or less than $1/\sigma_{\text{eff,DPS}}$) the contributions from the first term are also non-negligible.

$\Upsilon \Upsilon$) production is a typical channel for DPS studies in pp, given their large cross sections and relatively well-understood double-SPS backgrounds.^{73–75} In Ref.,²⁰ the DPS cross section for double- J/ψ production in PbPb collisions has been estimated via Eq. (55) with $m = 1$, $\sigma_{\text{eff,DPS,AA}} = 1.5 \pm 0.1$ nb, and prompt- J/ψ SPS cross section computed at NLO via CEM⁶⁵ with the CT10 proton and the EPS09 nuclear PDF, and theoretical scales $\mu_R = \mu_F = 1.5 m_c$ for a c -quark mass $m_c = 1.27$ GeV. The EPS09 nuclear modification factors result in a reduction of 20–35% of the J/ψ cross sections compared to those calculated using the free proton PDFs.

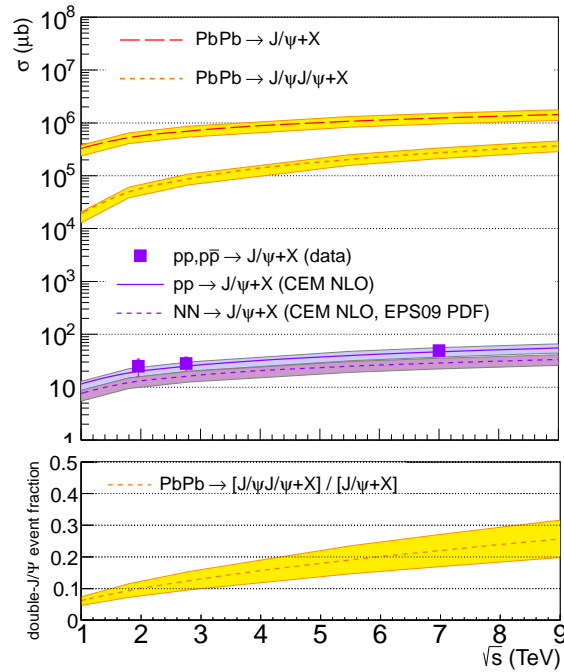


Fig. 7. Top: Production cross sections as a function of c.m. energy for prompt- J/ψ in pp, NN, and PbPb, and for DPS $J/\psi J/\psi$ in PbPb collisions. Bottom: Fraction of J/ψ events in PbPb collisions with a pair of J/ψ mesons produced, as a function of $\sqrt{s_{\text{NN}}}$. Bands show the nuclear PDF and scales uncertainties in quadrature. [Fig. from Ref.²⁰].

Figure 7 shows the \sqrt{s} -dependence of single- J/ψ in pp, NN and PbPb collisions (top panel), and of double- J/ψ cross sections in PbPb, as well as the fraction of J/ψ events with double- J/ψ produced via DPS (bottom panel). Our theoretical setup with CT10 (anti)proton PDF alone

agrees well with the experimental pp, $p\bar{p}$ data^{76–81} extrapolated to full phase space²⁰ (squares in Fig. 7). At the nominal PbPb energy of 5.5 TeV, the single prompt- J/ψ cross section is ~ 1 b, and $\sim 20\%$ of such collisions are accompanied by the production of a second J/ψ from a double parton interaction. Accounting for dilepton decays, acceptance and efficiency, which reduce the yields by a factor of $\sim 3 \cdot 10^{-7}$ in the ATLAS/CMS (central) and ALICE (forward) rapidities, the visible cross section is $d\sigma_{J/\psi, J/\psi}^{\text{DPS}}/dy|_{y=0,2} \approx 60$ nb, i.e. about 250 double- J/ψ events per unit-rapidity (both at central and forward y) are expected in the four combinations of dielectron and dimuon channels for a $\mathcal{L}_{\text{int}} = 1 \text{ nb}^{-1}$ integrated luminosity (assuming no net in-medium J/ψ suppression or enhancement).

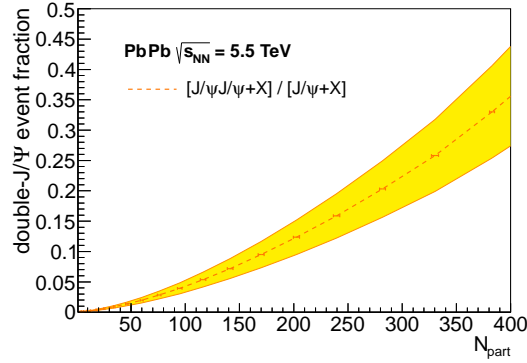


Fig. 8. Fraction of J/ψ events in PbPb collisions at 5.5 TeV where a J/ψ -pair is produced from double-parton scatterings as a function of the reaction centrality (given by N_{part}), as per Eq. (61). The band shows the EPS09 PDF plus scale uncertainties.²⁰

Following Eq. (61), the probability of $J/\psi J/\psi$ DPS production increases rapidly with decreasing impact parameter and $\sim 35\%$ of the most central $\text{PbPb} \rightarrow J/\psi + X$ collisions have a second J/ψ produced in the final state (Fig. 8). These results show quantitatively the large probability for double-production of J/ψ mesons in high-energy nucleus-nucleus collisions. Thus, the observation of a J/ψ pair in a given PbPb event should not be (blindly) interpreted as e.g. indicative of J/ψ production via $c\bar{c}$ regeneration in the QGP,⁸² since DPS constitute an important fraction of the inclusive J/ψ yield, with or without final-state dense medium effects.

Table 5 collects the DPS cross sections for the (pair) production of quarkonia (J/ψ , Υ) and/or electroweak bosons (W, Z) in PbPb collisions at

Double, triple, and n-parton scatterings in high-energy proton & nuclear collisions 27

the nominal LHC energy of 5.5 TeV, obtained via Eq. (55) with $\sigma_{\text{eff,DPS,AA}} = 1.5$ nb. The visible DPS yields for $\mathcal{L}_{\text{int}} = 1 \text{ nb}^{-1}$ are quoted taking into account $\text{BR}(J/\psi, \Upsilon, W, Z) = 6\%, 2.5\%, 11\%, 3.4\%$ per dilepton decay; plus simplified acceptance and efficiency losses: $\mathcal{A} \times \mathcal{E}(J/\psi) \approx 0.01$ (over 1-unit of rapidity at $|y| = 0$, and $|y| = 2$), and $\mathcal{A} \times \mathcal{E}(\Upsilon; W, Z) \approx 0.2; 0.5$ (over $|y| < 2.5$). All listed processes are in principle observable in the LHC heavy-ion runs, whereas rarer DPS processes like $W+Z$ and $Z+Z$ have much lower visible cross sections and would require much higher luminosities and/or c.m. energies such as those reachable at the FCC.

Table 5. Production cross sections at $\sqrt{s_{\text{NN}}} = 5.5$ TeV for SPS quarkonia and electroweak bosons in NN collisions, and for DPS double- J/ψ , $J/\psi + \Upsilon$, $J/\psi+W$, $J/\psi+Z$, double- Υ , $\Upsilon+W$, $\Upsilon+Z$, and same-sign WW , in PbPb. DPS cross sections are obtained via Eq. (55) for $\sigma_{\text{eff,DPS,AA}} = 1.5$ nb (uncertainties, not quoted, are of the order of 30%), and the corresponding yields, after dilepton decays and acceptance+efficiency losses (note that the J/ψ yields are *per unit of rapidity* at mid- and forward- y , see text), are given for the nominal 1 nb^{-1} integrated luminosity.

PbPb (5.5 TeV)	$J/\psi + J/\psi$	$J/\psi + \Upsilon$	$J/\psi+W$	$J/\psi+Z$
$\sigma_{\text{NN} \rightarrow a}^{\text{SPS}}, \sigma_{\text{NN} \rightarrow b}^{\text{SPS}}$	25 μb ($\times 2$)	25 μb , 1.7 μb	25 μb , 30 nb	25 μb , 20 nb
$\sigma_{\text{PbPb}}^{\text{DPS}}$	210 mb	28 mb	500 μb	330 μb
$N_{\text{PbPb}}^{\text{DPS}} (1 \text{ nb}^{-1})$	~ 250	~ 340	~ 65	~ 14
	$\Upsilon + \Upsilon$	$\Upsilon+W$	$\Upsilon+Z$	ss WW
$\sigma_{\text{NN} \rightarrow a}^{\text{SPS}}, \sigma_{\text{NN} \rightarrow b}^{\text{SPS}}$	1.7 μb ($\times 2$)	1.7 μb , 30 nb	1.7 μb , 20 nb	30 nb ($\times 2$)
$\sigma_{\text{PbPb}}^{\text{DPS}}$	960 μb	34 μb	23 μb	630 nb
$N_{\text{PbPb}}^{\text{DPS}} (1 \text{ nb}^{-1})$	~ 95	~ 35	~ 8	~ 15

5.2. TPS cross sections in AA collisions

For completeness, we estimate here the expected scaling of TPS cross sections in nucleus-nucleus compared to proton-proton collisions. Following our discussion for pA in Sec. 4.2, the TPS cross section in AA collisions results from the sum of nine terms, schematically represented in Fig. 9, generated by three independent structures appearing in triple parton scatterings in pA:

$$\begin{aligned} \sigma_{\text{AA} \rightarrow abc}^{\text{TPS}} \propto & A \cdot A + 3A \cdot A^2 + A \cdot A^3 \\ & + 3A^2 \cdot A + 9A^2 \cdot A^2 + 3A^2 \cdot A^3 \\ & + A^3 \cdot A + 3A^3 \cdot A^2 + A^3 \cdot A^3. \end{aligned} \quad (62)$$

These nine terms have different prefactors that can be expressed as a

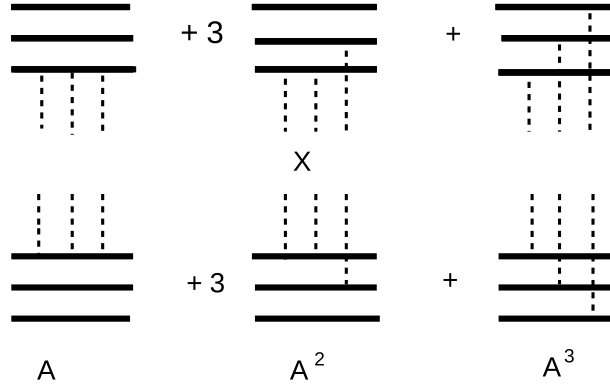


Fig. 9. Schematic diagrams contributing to TPS cross sections in AA collisions.

function of the nuclear thickness function, and the effective TPS and DPS cross sections, as done previously for the simpler pA case, see e.g. Eq. (38). For instance, the first $A \cdot A$ term is just the TPS cross section in NN collisions scaled by A^2 :

$$\sigma_{AA \rightarrow abc}^{\text{TPS},1} = A^2 \cdot \sigma_{NN \rightarrow abc}^{\text{TPS}}, \quad (63)$$

whereas the last $A^3 \cdot A^3$ contribution arises from interactions of partons from three different nucleons in one nucleus with partons from three different nucleons in the other nucleus (i.e. they result from triple *nucleon-nucleon* scatterings):

$$\sigma_{AA \rightarrow abc}^{\text{TPS},9} = \sigma_{NN \rightarrow abc}^{\text{TPS}} \cdot \sigma_{\text{eff,TPS}}^2 \cdot T_{9,AA}, \quad \text{with } T_{9,AA} = \int d^2r T_{AA}^3(\mathbf{r}). \quad (64)$$

In this latter expression, for simplicity, we omitted the $[(A-1)(A-2)/A^2]^2$ factor needed to account for the difference between the total number of nucleon triplets and that of different nucleon triplets. The ratio

$$\sigma_{AA \rightarrow abc}^{\text{TPS},1} / \sigma_{AA \rightarrow abc}^{\text{TPS},9} \approx [2 / \sigma_{\text{eff,DPS}} T_{AA}(0)]^2 \quad (65)$$

shows that the “pure” TPS contributions arising from partonic collisions within a single nucleus (which scale as A^2) are negligible compared to triple particle production coming from three independent nucleon-nucleon collisions which scale as $A^6 (r_p/R_A)^4 \propto A^{14/3}$. In the PbPb case, the relative weights of these two “limiting” TPS contributions are 1 : 40 000, to be compared with 1 : 200 for the similar DPS weights. The many other intermediate terms of Eq. (62) correspond to the various “mixed” parton-nucleon contributions, which can be also written in analytical form in this

Double, triple, and n-parton scatterings in high-energy proton & nuclear collisions 29

approach but, however, are suppressed by additional powers of A compared to the dominant nucleon-nucleon triple scattering.

Thus, as found in the DPS case, TPS processes in AA collisions are not so useful to derive $\sigma_{\text{eff,DPS}}$ or $\sigma_{\text{eff,TPS}}$ and thereby study the intranucleon partonic structure as in pp or pA collisions. The estimates presented here demonstrate that double- and triple- (hard) nucleon-nucleon scatterings represent a significant fraction of the inelastic hard AA cross section, and the standard Glauber MC provides a simpler approach to compute their occurrence in a given heavy-ion collision.

6. Summary

Multiparton interactions are a major contributor to particle production in proton and nuclear collisions at high center-of-mass energies. The possibility to concurrently produce multiple particles with large transverse momentum and/or mass in independent parton-parton scatterings in a given proton (nucleon) collision increases with \sqrt{s} , and provides valuable information on the badly-known 3D partonic profile of hadrons, on the unknown energy evolution of the parton density as a function of impact parameter b , and on the role of partonic spatial, momentum, flavour, colour,... correlations in the hadronic wave functions.

We have reviewed the factorized framework that allows one to compute the cross sections for the simultaneous perturbative production of particles in double- (DPS), triple- (TPS), and in general n -parton (NPS) scatterings, from the corresponding single-parton scattering (SPS) cross sections in proton-proton, proton-nucleus, and nucleus-nucleus collisions. The basic parameter of the factorized ansatz is an effective cross section parameter, σ_{eff} , encoding all unknowns about the underlying generalized n -parton distribution function in the proton (nucleon). In the simplest and most phenomenologically-useful approach, we have shown that σ_{eff} bears a simple geometric interpretation in terms of powers of the inverse of the integral of the hadron-hadron overlap function over all impact parameters. Simple recursive expressions can thereby be derived to compute the NPS cross section from the n -th product of the SPS ones, normalized by $n^{\text{th}-1}$ power of σ_{eff} . In the case of pp collisions, a particularly simple and robust relationship between the effective DPS and TPS cross sections, $\sigma_{\text{eff,DPS}} = (0.82 \pm 0.11) \times \sigma_{\text{eff,TPS}}$, has been extracted from an exhaustive analysis of typical parton transverse distributions of the proton, including those commonly used in Monte Carlo hadronic generators such as PYTHIA 8

and HERWIG++.

In proton-nucleus and nucleus-nucleus collisions, the parton flux is augmented by the number A and A^2 , respectively, of nucleons in the nucleus (nuclei). The larger nuclear transverse parton density compared to that of protons, results in enhanced probability for NPS processes, coming from interactions where the colliding partons belong to the same nucleon, and/or to two or more different nucleons. Whereas the standard SPS cross sections scale with the mass-number A in pA relative to pp collisions, we have found that the DPS and TPS cross sections are further enhanced by factors of order $(A + (1/\pi) A^{4/3})$ and $(A + (2/\pi) A^{4/3} + (1/\pi^2) A^{5/3})$ respectively. In the case of pPb collisions, this implies enhancement factors of ~ 600 (for DPS) and of ~ 1900 (for TPS) with respect to the corresponding SPS cross sections in pp collisions. The relative roles of intra- and inter-nucleon parton contributions to DPS and TPS cross sections in pA collisions have been also derived. In pPb, 1/3 of the DPS yields come from partonic interactions within just one nucleon of the Pb nucleus, whereas 2/3 involve scatterings from partons of two Pb nucleons; whereas for the TPS yields, 10% of them come from partonic interactions within one nucleon, 50% involve scatterings within two nucleons, and 40% come from partonic interactions in three different Pb nucleons. In proton-nucleus collisions, one can thereby exploit the large expected DPS and TPS signals over the SPS backgrounds to study double- and triple- parton scatterings in detail and, in particular, to extract the value of the key $\sigma_{\text{eff,DPS}}$ parameter independently of measurements in pp collisions, given that the corresponding NPS yields in pA depend on the comparatively better-known nuclear transverse density profile.

For heavy ions, the A^2 -scaling of proton-proton SPS cross sections becomes $\propto (A^2 + (2/\pi) A^{7/3} + 1/(2\pi) A^{10/3})$ for DPS cross sections, and includes much larger powers of A (up to $A^{14/3}$) for TPS processes. In the PbPb case, these translate into many orders-of-magnitude enhancements (e.g. the DPS cross sections are $\sim 10^7$ larger than the corresponding SPS pp ones). In addition, the MPI probability is significantly enhanced for increasingly central collisions: the impact-parameter dependence of DPS cross sections is basically proportional to the AA nuclear overlap function at a given b . The huge DPS and TPS cross sections expected in AA collisions are, however, clearly dominated by scatterings among partons of *different* nucleons, rather than by partons belonging to the same proton or neutron. For nuclei with mass numbers $A = 40$ –240, the relative weights of the three components contributing to DPS scattering in AA collisions are 1 : 2.3 : 23 (for $A = 40$) and 1 : 4 : 200 (for $A = 208$). Namely,

Double, triple, and n-parton scatterings in high-energy proton & nuclear collisions 31

only 13% (for $^{40}\text{Ca}+^{40}\text{Ca}$) or 2.5% (for $^{208}\text{Pb}+^{208}\text{Pb}$) of the DPS yields in AA collisions come from diagrams involving partons from one single nucleon. Clearly, the “pure” DPS contributions involving partonic collisions within a nucleon are much smaller than those issuing from two independent *nucleon-nucleon* collisions. In the TPS case, the relative weights of the two extreme contributions (three parton collisions within two single nucleons versus those from three different nucleon-nucleon collisions) are 1 : 40 000 for PbPb. The NPS cross sections in AA are practically unaffected by the value of $\sigma_{\text{eff,DPS}}$ and, although DPS and TPS processes account for a significant fraction of the inelastic hard AA cross section, they are not as useful as those in pp or pA collisions to study the partonic structure of the proton (nucleon).

Numerical examples for the cross sections and visible yields expected for the concurrent DPS and TPS production of heavy-quarks, quarkonia, and/or gauge bosons in proton and nuclear collisions at LHC, FCC, and at ultra-high cosmic-ray energies have been provided. The obtained DPS and TPS cross sections are based on perturbative QCD predictions for the corresponding single inclusive processes at NLO or NNLO accuracy including, when needed, nuclear modifications of the corresponding parton densities. Processes such as double- J/ψ , $J/\psi \Upsilon$, $J/\psi W$, $J/\psi Z$, double- Υ , ΥW , ΥZ , and same-sign $W W$ production have large cross sections and visible event rates for the nominal LHC and FCC luminosities. The study of such processes in proton-nucleus collisions provides an independent means to extract the effective $\sigma_{\text{eff,DPS}}$ parameter characterising the transverse parton distribution in the nucleon. In addition, we have shown that double- J/ψ and double- Υ final states have to be explicitly taken into account in any event-by-event analysis of quarkonia production in heavy-ion collisions. The TPS processes, although not observed so far, have visible cross sections for charm and bottom in pp and pA collisions at LHC and FCC energies. At the highest c.m. energies reached in collisions of cosmic rays with the nuclei in the upper atmosphere, the TPS cross section for triple charm-pair production equals the total p-Air inelastic cross section, indicating that *all* such collisions produce at least three $c\bar{c}$ -pairs in multiple partonic interactions. The results presented here emphasize the importance of having a good understanding of the NPS dynamics in hadronic collisions at current and future colliders, both as genuine probes of QCD phenomena and as backgrounds for searches of new physics in rare final-states with multiple heavy-particles, and their relevance in our comprehension of ultrarelativistic cosmic-ray interactions with the atmosphere.

References

1. T. Sjöstrand and M. van Zijl, Phys. Rev. D **36** (1987) 2019
2. P. Bartalini *et al.*, arXiv:1111.0469 [hep-ph]
3. H. Abramowicz *et al.*, arXiv:1306.5413 [hep-ph]
4. S. Bansal *et al.*, arXiv:1410.6664 [hep-ph]
5. R. Astalos *et al.*, arXiv:1506.05829 [hep-ph]
6. H. Jung, D. Treleani, M. Strikman and N. van Buuren, DESY-PROC-2016-01
7. M. Strikman and D. Treleani, Phys. Rev. Lett. **88** (2002) 031801
8. A. Del Fabbro and D. Treleani, Phys. Rev. D **70** (2004) 034022
9. L. Frankfurt, M. Strikman and C. Weiss, Annalen Phys. **13** (2004) 665
10. E. Cattaruzza, A. Del Fabbro and D. Treleani, Phys. Rev. D **70** (2004) 034022
11. A. Del Fabbro and D. Treleani, Eur. Phys. J. A **19S1** (2004) 229
12. E. Cattaruzza, A. Del Fabbro and D. Treleani, IMPA **20** (2005) 4462
13. D. Treleani and G. Calucci, Phys. Rev. D **86** (2012) 036003
14. B. Blok, M. Strikman and U.A. Wiedemann, Eur. Phys. J. C **73** (2013) 2433
15. D. d'Enterria and A. M. Snigirev, Phys. Lett. B **718** (2013) 1395
16. S. Salvini, D. Treleani and G. Calucci, Phys. Rev. D **89** (2014) 016020
17. D. d'Enterria and A. M. Snigirev, Nucl. Phys. A **931** (2014) 303
18. D. d'Enterria and A. M. Snigirev, Nucl. Phys. A **932** (2014) 296
19. D. d'Enterria and A. M. Snigirev, arXiv:1612.08112 [hep-ph]
20. D. d'Enterria and A. M. Snigirev, Phys. Lett. B **727** (2013) 157
21. T. Sjöstrand, arXiv:1706.02166 [hep-ph]
22. D. d'Enterria *et al.*, Eur. Phys. J. C **66** (2010) 173
23. V. Khachatryan *et al.* [CMS Collaboration], JHEP **1009** (2010) 091
24. G. Aad *et al.* [ATLAS Collaboration], Phys. Rev. Lett. **116** (2016) 172301
25. F. Abe *et al.* [CDF Collaboration], Phys. Rev. D **56** (1997) 3811
26. F. Abe *et al.* [CDF Collaboration], Phys. Rev. Lett. **79** (1997) 584
27. V. M. Abazov *et al.* [D0 Collaboration], Phys. Rev. D **89** (2014) 072006
28. V. M. Abazov *et al.* [D0 Collaboration], Phys. Rev. D **93** (2016) 052008
29. M. Aaboud *et al.* [ATLAS Collaboration], JHEP **1611** (2016) 110
30. M. Aaboud *et al.* [ATLAS Collaboration], Eur. Phys. J. C **77** (2017) 76
31. S. Chatrchyan *et al.* [CMS Collaboration], JHEP **1403** (2014) 032
32. V. Khachatryan *et al.* [CMS Collaboration], Eur. Phys. J. C **76** (2016) 155
33. R. Aaij *et al.* [LHCb Collaboration], JHEP **07** (2016) 052
34. D. d'Enterria and A. M. Snigirev, Phys. Rev. Lett. **118** (2017) 122001
35. M. L. Mangano *et al.*, CERN Yellow Report (2017) no.3, 1
36. A. Dainese *et al.*, CERN Yellow Report (2017) no.3, 635
37. J. C. Collins, D. E. Soper and G. F. Sterman, Adv. Ser. Direct. High Energy Phys. **5** (1989) 1
38. A.M. Snigirev, Phys. Rev. D **94** (2016) 034026
39. T. Sjöstrand, S. Mrenna and P. Z. Skands, Comput. Phys. Commun. **178** (2008) 852.
40. M. H. Seymour and A. Siodmok, JHEP **10** (2013) 113
41. B. Blok, Yu. Dokshitzer, L. Frankfurt, and M. Strikman, Phys. Rev. D **83** (2011) 071501

Double, triple, and n-parton scatterings in high-energy proton & nuclear collisions 33

42. See other chapters of this report.
43. M. Luszczak, R. Maciula, and A. Szczurek, Phys. Rev. D **85** (2012) 094034
44. A.V. Berezhnoy *et al.*, Phys. Rev. D **86** (2012) 034017
45. E.R. Cazaroto, V.P. Goncalves, F.S. Navarra, Phys. Rev. D **88** (2013) 034005
46. R. Maciula and A. Szczurek, arXiv:1703.07163 [hep-ph]
47. David d'Enterria, Proceeds. Moriond-QCD (2017), to be submitted.
48. M. Czakon, P. Fiedler and A. Mitov, Phys. Rev. Lett. **110** (2013) 252004
49. S. Alekhin, J. Bluemlein, S.O. Moch, R. Placakyte, arXiv:1609.03327 [hep-ph]
50. M. Cacciari *et al.*, JHEP **10** (2012) 137
51. M. L. Mangano, P. Nason and G. Ridolfi, Nucl. Phys. B **373** (1992) 295
52. D. d'Enterria and T. Pierog, JHEP **08** (2016) 170
53. N. Armesto, J. Phys. G **32** (2006) R367
54. D. d'Enterria, nucl-ex/0302016.
55. C.W. deJager, H. deVries, and C. deVries, Atomic Data and Nuclear Data Tables **14** (1974) 485
56. A. Kulesza and W.J. Stirling, Phys. Lett. B **475** (2000) 168
57. <http://mcfm.fnal.gov>
58. J. Campbell, R.K. Ellis and C. Williams, JHEP **1107** (2011) 018
59. H.-L. Lai *et al.*, Phys. Rev. D **82** (2010) 074024
60. K. J. Eskola, H. Paukkunen and C. A. Salgado, JHEP **0904** (2009) 065
61. <http://www-itp.particle.uni-karlsruhe.de/vbfnlo>
62. K. Arnold *et al.*, arXiv:1207.4975 [hep-ph]
63. H. Paukkunen and C. A. Salgado, JHEP **1103** (2011) 071
64. T. Melia, K. Melnikov, R. Rontsch, G. Zanderighi, JHEP **1012** (2010) 053
65. R. Vogt, R. E. Nelson and A. D. Frawley, Nucl. Phys. A **910-911** (2013) 231
66. J. Adam *et al.* [ALICE Collaboration], Phys. Rev. C **94** (2016) 054908
67. K. Greisen, Phys. Rev. Lett. **16** (1966) 748.
68. G. T. Zatsepin and V. A. Kuzmin, JETP Lett. **4** (1966) 78 [Pisma Zh. Eksp. Teor. Fiz. **4** (1966) 114].
69. D. d'Enterria, R. Engel, T. Pierog, S. Ostapchenko and K. Werner, Astropart. Phys. **35** (2011) 98
70. I. P. Lokhtin and A. M. Snigirev, Eur. Phys. J. C **16** (2000) 527
71. T. Matsui and H. Satz, Phys. Lett. B **178** (1986) 416
72. J. P. Lansberg *et al.*, AIP Conf. Proc. **1038** (2008) 15
73. S. P. Baranov, A. M. Snigirev, N. P. Zotov, A. Szczurek and W. Schäfer, Phys. Rev. D **87** (2013) 034035
74. J. P. Lansberg and H. S. Shao, Phys. Lett. B **751** (2015) 479
75. L. P. Sun, H. Han and K. T. Chao, Phys. Rev. D **94** (2016) 074033
76. D. Acosta *et al.* [CDF Collaboration], Phys. Rev. D **71** (2005) 032001
77. B. Abelev *et al.* [ALICE Collaboration], Phys. Lett. B **718** (2012) 295
78. R. Aaij *et al.* [LHCb Collaboration], JHEP **1302** (2013) 041
79. B. Abelev *et al.* [ALICE Collaboration], JHEP **1211** (2012) 065
80. V. Khachatryan *et al.* [CMS Collaboration], Eur. Phys. J. C **71** (2011) 1575
81. R. Aaij *et al.* [LHCb Collaboration], Eur. Phys. J. C **71** (2011) 1645
82. A. Andronic, P. Braun-Munzinger, K. Redlich and J. Stachel, J. Phys. G **37** (2010) 094014